How competition shapes energy efficiency in shared e-scooter systems

Transportation Research Part D 157 (2026) 105427

Contents lists available at ScienceDirect

Transportation Research Part D

journal homepage: www.elsevier.com/locate/trd

How competition shapes energy efficiency in shared e-scooter systems

Yuhan Zhang [a], Jiaming Wu [b,*], Zhirui Ye [a], Maria Attard [c]

[a] School of Transportation, Southeast University, Nanjing, China
[b] Architecture and Civil Engineering, Chalmers University of Technology, Gothenburg, Sweden
[c] Institute for Climate Change and Sustainable Development, University of Malta, Msida, MSD2080, Malta

ARTICLE INFO

Keywords:
Shared e-scooter systems
competition
energy consumption
spatial heterogeneity
explainable machine learning

ABSTRACT

Shared e-scooter systems provide a flexible and sustainable solution for short urban trips. However, low operational efficiency often results in long idle periods, during which e-scooters waste energy without providing service. This study investigates how excessive inter-operator competition is associated with such inefficiencies. Using high-resolution operational data from Parma, Italy, where two operators coexisted, we reconstruct full lifecycles and introduce a novel entropy-based competition index. We use an interpretable machine learning framework to assess how competition factors relate to idle energy consumption. The results show that competition-related patterns are associated with higher idle energy consumption, with relocation-based rivalry being most informative for the non-dominant operator. For the weaker operator, over half of battery discharge occurs while idle, with competition accounting for about 70% of the total SHAP importance. These findings call for demand-responsive fleet management and context-sensitive regulation to reduce unnecessary competition and support sustainable micromobility.

1. Introduction

Shared e-scooters are now a popular member of urban mobility, effectively serving last-mile trips and complementing public transit networks (Guo and Zhang, 2021; Zhang et al., 2021; Badia and Jenelius, 2023; Huang et al., 2024; Yang and Ewing, 2024). In the United States, over 300 e-scooter systems operated across 158 cities as of 2022 (Verma and McKenzie, 2024), while globally, the market was valued at approximately USD 1.9 billion in 2024 and is projected to grow by nearly 5.7% to over USD 2 billion in 2025 (Statista Research Department, 2025). Within the micromobility sector, e-scooters are establishing a dominant position, highlighting their growing importance in sustainable urban transport (Towards Automotive, 2025).

Over the years, the shared e-scooter market has evolved rapidly under fierce competition. Operators are driven to develop safer and smarter vehicles. For example, Voi in Europe has just launched its eighth generation e-scooters within seven short years. Cities have likewise shifted from initial enthusiasm, to periods of clampdowns, and more recently to organized tenders[1]. The dynamic market has seen hundreds of companies emerge, boom, and in many cases, exit. In parallel, numerous studies have investigated the new mode of travel, focusing primarily on the travel patterns, economic perspectives, and operational system optimization

* Corresponding author at: Department of Architecture and Civil Engineering, Chalmers University of Technology, Sven Hultins gata 6 SE-412 96, Gothenburg, Sweden
E-mail addresses: yuhanzhang@seu.edu.cn (Y. Zhang), jiaming.wu@chalmers.se (J. Wu).
URL: https://research.chalmers.se/en/person/jiwu (J. Wu)

[1] In this context, “tender” refers to a formal bidding process organized by city authorities to select or regulate shared e-scooter operators.

https://doi.org/10.1016/j.trd.2026.105427
Received 7 October 2025; Received in revised form 7 May 2026; Accepted 7 May 2026
Available online 20 May 2026

(Kimpton et al., 2022; Jin et al., 2023; Fuady et al., 2024; Zhai et al., 2025). However, energy perspectives have been overlooked, despite evidence indicating that up to 40% of e-scooter battery energy can be wasted in daily operations (Wang et al., 2021; Al-Habaibeh et al., 2024).

E-scooter batteries are depleted not only during trips but also while idling, as sensors, GPS modules, and lighting systems remain active. This idle consumption is inherently inefficient, as it generates neither mobility services nor operator revenue. Evaluating such inefficiency is particularly important given the large fleet sizes and, collectively, the substantial battery stock across cities (Huang et al., 2016; Bozzi and Aguilera, 2021; Emami and Ramezani, 2024). While the capacity of a single battery may appear small, the aggregate idle losses of entire fleets are nontrivial. Since the duration of idling depends on the frequency of usage, it is thus natural to link energy efficiency to usage rate, where the competition between co-existing operators plays a key role. As competition is the defining feature of the market, this study, for the first time, examines how competition is associated with idle energy consumption, accounting for geographic characteristics, built environment, temperature, and temporal variations.

Addressing this problem is complex due to both analytical and empirical challenges. From a theoretical perspective, a clear definition of competition and suitable models have not been established in the literature. This is difficult because energy efficiency or usage rates are jointly shaped by both operators and users. Analyzing competition therefore requires careful isolation of user-related factors. From an empirical perspective, robust conclusions demand multi-operator data, yet most existing studies rely on datasets from a single provider (Zhu et al., 2022; Jiao et al., 2024a), limiting their insights into competitive dynamics. The scarcity of comprehensive multi-operator datasets has thus hindered research in this area.

To overcome these limitations, we conceptualize operators' competition through two dimensions: the initial fleet deployment and daily operational activities. Fleet size reflects operators' long-term commitment, whereas daily operations, including relocation, charging, and maintenance are active actions to improve competitiveness. This study focuses on dockless shared e-scooters, which are free-floating and can be parked within designated public areas. This operational model differs from dock-based systems and better reflects the current dominant practice in European cities, including Parma. Real-world data from Parma are utilized in this research, a city where two operators initially coexisted as sole providers before one exited the market. This unique dataset allows us to compare competitive and non-competitive market conditions within the same urban context. A spatial analysis approach is adopted to ensure sufficient granularity and to capture the dynamic spatiotemporal patterns of competition across different regions of the city. We then apply interpretable machine learning models to examine how competition, together with contextual and operational factors, shapes idle energy consumption through complex, nonlinear relationships. The tailored machine learning model, though largely standard in structure, yields robust and interpretable results that uncover hidden competition patterns. Overall, this study contributes to the literature by offering a novel energy-oriented perspective grounded in real-world evidence, rather than by advancing methodological innovations. Specifically, the contributions of this study are summarized as follows:

- we provide the first systematic analysis of how inter-operator competition is associated with idle-state operational efficiency in shared e-scooter systems, addressing a critical yet understudied dimension of market dynamics.
- we leverage a unique multi-operator dataset from Parma, covering both competitive and non-competitive periods, to enable robust empirical investigation of associational patterns related to competition.
- we introduce an energy-focused perspective by quantifying idle energy consumption as a proxy for system inefficiency, offering operational and policy implications for the environmental sustainability of shared e-scooter operations.

The rest of the paper is organized as follows. Section 2 reviews data-driven research on shared e-scooters, focusing on three main areas: user behavior, operational strategies, and system impact evaluation. Section 3 outlines the methodological framework based on interpretable machine learning. Section 4 presents the case study data and its results. Section 5 discusses key insights and policy implications. Finally, Section 6 summarizes the conclusions of the study.

2. Literature Review

Market competition among shared e-scooter providers is shaped by user behavior and mobility patterns, providers' operational strategies, and the characteristics of the built environment (Huo et al., 2021; Yang et al., 2022b). Although relatively few studies explicitly focus on multi-operator competition mechanisms, a broad and fast-growing body of data-driven research provides useful methods and findings that inform how demand, supply operations, and system-level outcomes interact in shared e-scooter markets. To position this study within the existing evidence, we organize the related literature into three connected streams: (i) user behavior and demand patterns, (ii) operator strategies, fleet management, and operational efficiency, and (iii) system-level impacts and policy evaluation. This organization aligns with our study logic: demand conditions and urban context shape where scooters are used, while operational decisions shape how fleets are deployed, relocated, and charged; together these processes are associated with system outcomes that matter to cities and regulators.

2.1. User behavior and demand patterns

Understanding user behavior and demand patterns is crucial for both providers and cities, because demand regularities determine when and where supply shortages emerge and therefore when operational interventions are likely to occur. Existing studies primarily utilize survey and trip data to build statistical and machine learning models that identify behavioral determinants and characterize spatiotemporal usage patterns. For example, Yang et al. (2022a) investigated how road features are associated with e-scooter trip

volume and found that facilitating infrastructure such as sidewalks and dedicated bicycle lanes is associated with higher usage. Trip-based spatiotemporal analyses also document strong heterogeneity across neighborhoods and time of day, and they often compare scooters with other shared modes to reveal systematic differences in usage patterns (McKenzie, 2019). Spatial association models based on dockless trip records further show that built-environment correlates such as land use and accessibility are strongly linked to where e-scooters are used (Caspi et al., 2020).

Beyond trip records, survey-based research provides complementary evidence on adoption, substitution, and perceived benefits. Budnitz et al. (2025) analyzed e-scooter trip data from Bristol using a negative binomial regression model and found that socioeconomic barriers are associated with lower access and adoption in high-deprivation neighborhoods, despite strong interest among younger and minority populations. In a Swedish web-based survey, Kazemzadeh and Sprei (2024) examined modal shift and reported that e-scooter riders typically have well-paid jobs, hold driver's licenses, and own multiple mobility resources such as e-bikes, cars, and transit cards. Contreras Pinochet et al. (2025) collected survey data in São Paulo and estimated a structural equation model with a necessary conditions analysis method, suggesting that users perceive shared e-scooters as particularly beneficial for short-distance travel. Related evidence indicates that perceived utility and green awareness (Yang et al., 2025), supportive street environments (Cao, 2025; Hu et al., 2024), spatial configuration of road infrastructure (Schumann et al., 2025), and non-commuting trip purposes (Chen et al., 2025) are associated with higher e-scooter usage. Using Seoul data, Kim et al. (2025) reports that public transport infrastructure and commuting population size are significantly associated with e-scooter demand, while Jiao et al. (2024b) shows that in areas with low population density and limited employment opportunities, e-scooters may be less attractive relative to ride-sourcing services.

Overall, the demand literature provides a strong empirical basis for understanding when and where e-scooters are used and how infrastructure, socioeconomic context, and built environment are associated with usage. However, because most studies rely on trip and survey data, they often do not observe the full operational lifecycle outside of trips, such as idle periods, relocation movements, and charging activities. This limitation is directly relevant to our study because idle processes and competition-related operational adjustments are not fully identifiable from trips alone, while these processes are central for understanding idle energy consumption.

2.2. Operator strategies, fleet management, and operational efficiency

On the supply side, operational strategies such as fleet sizing, rebalancing, and spatial configuration shape both revenue and operating costs (Zhang et al., 2023). Using fixed-effects regression with e-scooter trip datasets in Nashville, Shah et al. (2023) found that large-fleet operators exhibit substantially higher demand elasticity for deployment than medium-fleet providers, implying that fleet size decisions can materially affect observed performance. Wu et al. (2024) studied fleet sizing and static rebalancing strategies using heuristic algorithms and e-scooter trip data in Indianapolis, and found that operating with the minimum feasible fleet size can markedly reduce rebalancing distance costs compared to current fleet levels.

A closely related line of work develops optimization models that jointly consider rebalancing and energy-related operations. Osorio et al. (2021) studied optimal rebalancing with on-board charging for shared electric scooters and highlighted how charging logistics and rebalancing policies interact in determining system performance. More recent work also considers logistics choices such as battery swapping, vehicle rebalancing, and staff routing (Lee et al., 2024). These operational studies emphasize that system performance depends not only on where vehicles are demanded, but also on how operators reposition, charge, and maintain fleets under practical constraints.

Battery energy consumption is a crucial determinant of cost and sustainability, and it can vary with weather, infrastructure, and operational context. Gioldasis et al. (2024) applied linear regression to e-scooter GPS trajectory data and found that weather conditions and air temperature are significant predictors of battery energy consumption. At a broader level, evidence from life-cycle and environmental impact assessments highlights that operational practices such as collection, charging logistics, and maintenance can contribute materially to total environmental impacts (Hollingsworth et al., 2019). Reviews also synthesize how usage patterns and system design relate to user perceptions and environmental outcomes (Badia and Jenelius, 2023).

In summary, the operations literature demonstrates that fleet management and energy-related decisions are fundamental to shared e-scooter efficiency and cost. At the same time, empirically characterizing energy inefficiency processes at fine spatial and temporal scales remains challenging when only trip records are available. This challenge can be more pronounced in markets with multiple operators, because strategic behavior under competition can change relocation intensity, idle durations, and charging operations, which may be associated with idle energy consumption in ways that cannot be inferred from demand patterns alone.

2.3. System-level impacts and policy evaluation

Evaluating system-level impacts of shared e-scooters by examining supply levels, operational strategies, and user behavior helps policymakers and service providers understand diverse effects on urban mobility and welfare. Regarding integration with public transit, existing evidence shows that integration ratios vary substantially across cities (Li et al., 2024). A case study in Gothenburg suggests that shared e-scooters can enhance public transport accessibility within a 30-minute travel time (Hu et al., 2025). Other evidence indicates that e-scooter trip ends can cluster in areas with high-quality transit service, which may imply substitution or competition with transit in some contexts, while in other contexts such as nights, early mornings, weekends, and regions with poor rail access, e-scooters can provide a stronger first- and last-mile function (Currie et al., 2025). Related work evaluates whether and when e-scooters can enhance public transit use and reduce driving, highlighting that these patterns depend on local context and traveler behavior (Yan et al., 2023).

Equity and availability have also become central topics in policy evaluations. Abouelela et al. (2024) assessed shared e-scooter equity by simulating multiple scenarios and found that e-scooters can enhance accessibility in a subset of cases, often by substituting for walking, cycling, or public transit trips. Karimi and Kluger (2025) proposed a data-driven framework to evaluate equity across availability-based and distributive dimensions, showing that low-income and low-car-ownership neighborhoods may benefit from higher scooter availability, whereas majority-minority areas can experience rapid rebalancing and removal that limits local access. Zhao et al. (2024) further found that fleet unavailability under realistic demand and battery constraints can far exceed simple charge-level thresholds, and that land-use patterns and pedestrian access distances shape e-scooter availability.

Taken together, the literature provides substantial evidence on demand correlates, operational decision making, and system-level outcomes. However, important gaps remain for explaining operational inefficiency in realistic markets. First, although competition among multiple service providers is a defining feature of many shared e-scooter programs, empirical evidence on how competition is associated with operator behavior remains limited, in part because this question requires observing operator-specific deployments and relocations at fine spatiotemporal scales. Second, despite the central role of battery energy in operating cost and sustainability, prior work offers limited empirical evidence on how idle energy consumption varies across space and time and how such patterns are associated with competitive operational dynamics. Motivated by these limitations, our study uses multi-operator operational records to characterize competitive market structure and examines how competition measures co-vary with idle energy consumption, thereby complementing demand-focused and policy-focused evidence with a more operationally grounded understanding of energy inefficiency in shared e-scooter systems.

3. Methodology

This section presents the methodological framework developed to characterize the association between inter-operator competition and idle energy consumption in shared e-scooter systems. We introduce a novel competition index derived from relocation patterns and construct explanatory variables to capture spatial, temporal, and operational dynamics. Leveraging interpretable machine learning, we model nonlinear associations between competition and idle energy consumption. This methodological design is essential to overcome the limitations of traditional linear models, enabling a nuanced analysis of complex operational interactions in multi-operator urban mobility markets.

3.1. Framework

The data processing workflow is summarized in the conceptual framework presented in Fig. 1. We process raw e-scooter records into lifecycle data by classifying each time interval for every unique e-scooter into one of five operational states: idle, ride, relocation, charging, and deactivation[2]. The idle state refers to the period when an e-scooter remains stationary between two consecutive ride requests.In this paper, idle energy consumption denotes the battery energy depletion that occurs while a scooter remains stationary between rides during an idle interval. In our dataset it is operationalized using changes in battery state of charge (SOC) and is reported in SOC percentage points. During this period, idle energy consumption is quantified using SOC depletion observed over each idle interval, and we summarize it at the region–day level using the mean SOC loss per idle event as a micro-scale indicator of operational inefficiency.

Idle energy consumption is associated with both contextual and operational factors. At its core, it reflects a local mismatch between supply and demand. When supply exceeds demand, idle events become more frequent and last longer. In contrast, when demand is high, e-scooters are used more quickly, which is typically accompanied by fewer and shorter idle periods. Demand is not directly observed at the H3 cell-day level because the raw feed captures scooter availability states rather than latent trip requests. We therefore represent local activity intensity using fine-grained proxies available at the same spatial resolution as our H3 grid. In medium-sized European cities like Parma, official socioeconomic data such as population density, employment intensity, or income are typically released at coarse administrative units. Downscaling these layers to H3 Resolution 9 hexagons would introduce substantial spatial interpolation error. Given this constraint, we rely on Point-of-Interest (POI) density and distance to the city center. POI density is a widely accepted proxy in micromobility studies for capturing the fine-grained concentration of trip attractors like retail and services (Caspi et al., 2020; Abouelela et al., 2023; Heumann et al., 2021). Distance to the city center effectively captures the centrality gradient of activity intensity typical of Parma's urban structure (Abouelela et al., 2023). Supply is represented not only by user-driven trip destinations but also by operator-driven activities such as initial deployment and relocation.

To examine the competitive behavior among coexisting operators, two operator-related variables are central to the analysis: fleet deployment and relocation activity. Fleet size reflects the baseline deployment and remains relatively stable over time, whereas relocation is flexible and can be adjusted in real time to improve coverage and utilization. In practice, standard relocations, battery-swap charging, and deactivation events all involve repositioning, so the endpoints of these activities are treated collectively as relocation destinations. While competition captures the degree to which multiple operators simultaneously target the same spatial units, exclusivity can be understood as its limiting case, where relocation activities in a unit are dominated entirely by a single operator.

[2] Deactivation refers to periods when a scooter is deliberately taken out of service by the operator, for example due to maintenance, regulation, or market exit.

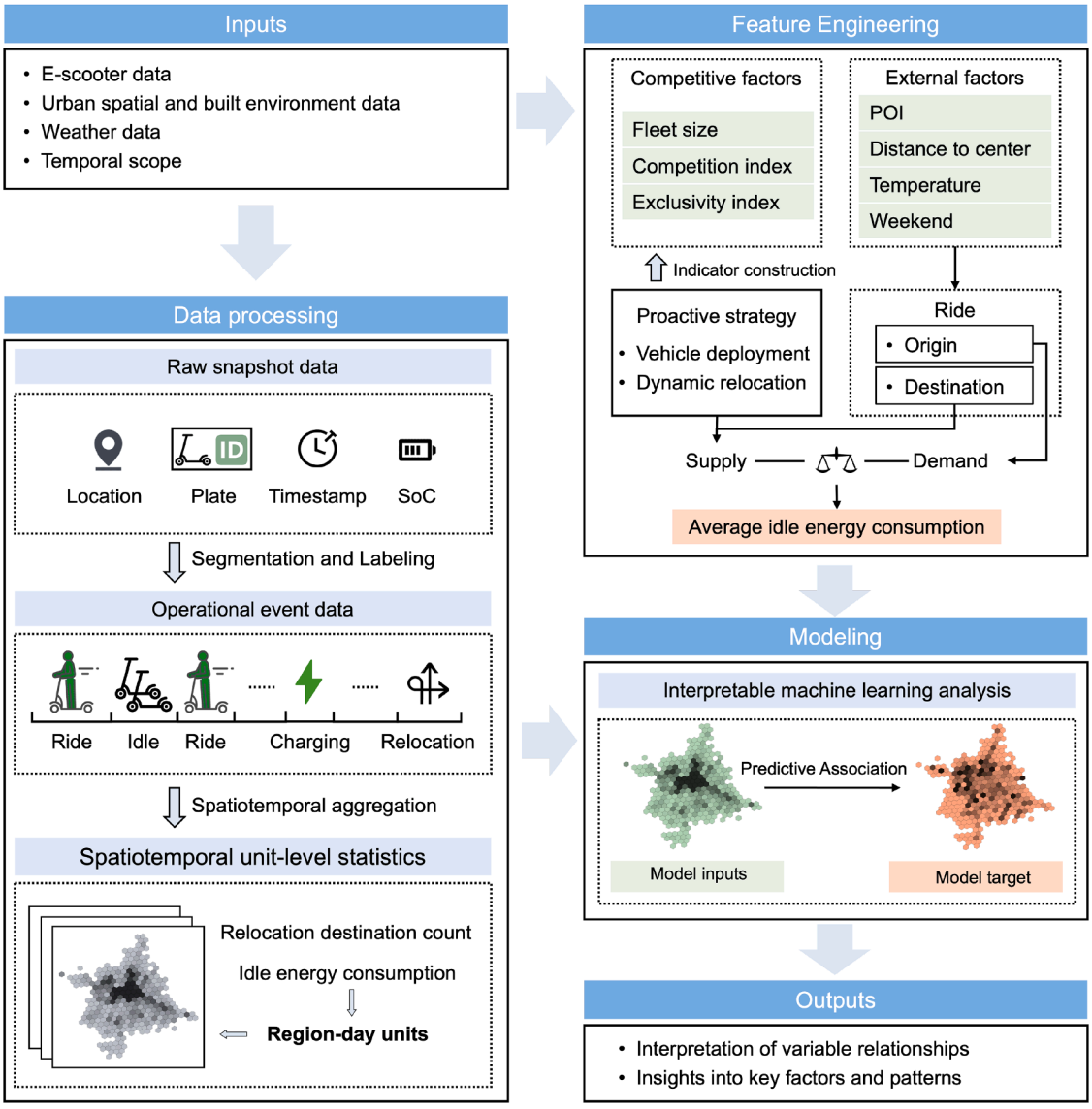

Fig. 1. Conceptual framework for idle energy consumption analysis.

Because relocation operations are inherently spatial and cross-zonal, the urban study area is partitioned into regular hexagonal cells using the H3 geospatial indexing system. By pairing each cell $z \in \mathcal{Z}$ with each day $d \in \mathcal{D}$, we define spatiotemporal units

$$u = (z, d) \in \mathcal{U} := \mathcal{Z} \times \mathcal{D}, \tag{1}$$

where $z \in \mathcal{Z}$ denotes an H3 cell in the study area, $d \in \mathcal{D}$ denotes a calendar day in the observation window, and $\mathcal{U}$ is the set of all cell–day units used in the analysis. For each vehicle $v \in \mathcal{V}$, the lifecycle is formulated as an ordered sequence of events:

$$L_v = \left\{ e_1^v, e_2^v, \ldots, e_{n_v}^v \right\}. \tag{2}$$

where $v \in \mathcal{V}$ indexes e-scooters, n_v is the number of observed events for vehicle v, and e_i^v denotes the i-th operational event in the reconstructed lifecycle. Each event e_i^v is a tuple of attributes, and is assigned to a unique region-day unit according to the geographical location of its start point and the timestamp of its occurrence.

$$e_i^v = \left(t_s, t_e, \boldsymbol{x}_s, \boldsymbol{x}_e, \mathrm{SOC}_i^s, \mathrm{SOC}_i^e, \tau_i\right),$$

where t_s, t_e denote start and end timestamps, $\boldsymbol{x}_s, \boldsymbol{x}_e$ the start and end geographic coordinates, $\mathrm{SOC}_i^s, \mathrm{SOC}_i^e$ the state-of-charge levels, and τ_i the event type.

We define a mapping from events to spatiotemporal units:

$$\phi : \mathcal{E} \to \mathcal{U}, \quad \phi(e_i^v) = \left(\mathrm{H3}(\boldsymbol{x}_s),\ \mathrm{Date}(t_s)\right). \tag{3}$$

where $\mathcal{E}$ is the set of reconstructed events; $\phi(\cdot)$ maps an event to its associated spatiotemporal unit; $\mathrm{H3}(\boldsymbol{x}_s)$ returns the H3 cell containing the event start location $\boldsymbol{x}_s$; and $\mathrm{Date}(t_s)$ returns the calendar date of the start timestamp t_s. Thus, each event belongs uniquely to a unit

$$e_i^v \in E_u \quad \text{if} \quad \phi(e_i^v) = u,$$

where $E_u \subseteq \mathcal{E}$ is the set of events associated with unit u. Accordingly, a lifecycle L_v can be expressed as a path across units:

$$L_v = \left(e_1^v \in E_{u_1},\ e_2^v \in E_{u_2}, \dots, e_{n_v}^v \in E_{u_{n_v}}\right).$$

For each unit $u = (z, d) \in \mathcal{U}$, we calculate a set of aggregated indicators capturing scooter activity levels, energy usage patterns, and operator deployment behaviors. Of particular interest is idle energy consumption during idle intervals. We define the dependent variable as the mean SOC loss per idle event in unit u:

$$Y^u = \frac{1}{N^u_{\text{idle}}} \sum_{e_i \in \text{Idle}(u)} \left|\,\text{SOC}_i^s - \text{SOC}_i^e\right|, \tag{4}$$

where $\text{Idle}(u) \subseteq E_u$ denotes the subset of idle events within unit u, and $N^u_{\text{idle}} = |\text{Idle}(u)|$ is the number of idle events in u. For each idle event i, SOC_i^s and SOC_i^e are the state-of-charge (SOC) values at the start and end of the idle interval, respectively.

The outcome Y^u is a conditional micro-scale inefficiency measure: it characterizes the typical SOC depletion during an idle spell in a given location–day context, conditional on an idle event occurring. It should not be interpreted as the total idle energy burden in unit u. A unit can have a moderate per-idle value but still accumulate a large total idle loss if idle exposure is high (many idle events and/or long idle time), and conversely a unit can have a high per-idle value but contribute less to total burden if idle events are rare. For transparency, we treat N^u_{idle} as an explicit exposure indicator and report it alongside the dependent variable when interpreting results. Since SOC loss is measured across the full idle interval, heterogeneity in idle duration is reflected in the observed per-event SOC loss rather than being ignored by construction.

SOC is adopted as the primary indicator because it is the standardized BMS-reported metric directly linked to the battery's open-circuit voltage (OCV), providing a consistent measure of relative energy change across models and health states (Xiong et al., 2017). Expressing energy in Wh would require model-specific capacity assumptions; for intuition, a 1% SOC decrease in typical shared e-scooters (0.3-1.0 kWh packs) corresponds to roughly 3-10 Wh of energy loss (Segway Inc., 2020; Electric-Scooter.Wiki Community, 2024).

To quantify competitive dynamics between operators, we consider the distribution of relocation endpoints in each spatiotemporal unit $u = (z, d)$. Let n_j^u denote the number of relocation endpoints attributed to operator j in unit u. Because entropy-based share measures can be unstable when relocation activity is extremely sparse, we introduce an activity threshold to define the active operator set $\mathcal{J}_u$ and the active operator count M^u:

$$\mathcal{J}_u = \{j : n_j^u \geq n_{\min}\}, \qquad M^u = |\mathcal{J}_u|. \tag{5}$$

where $n_{\min} = 2$ is the minimum number of endpoints required for an operator to be considered active in the unit, used to reduce noise from sporadic events; and M^u is the number of operators meeting this threshold.

For units with meaningful competition ($M^u \geq 2$), operator-specific relocation shares are defined over this active set:

$$p_j^u = \frac{n_j^u}{\sum_{k \in \mathcal{J}_u} n_k^u}, \qquad j \in \mathcal{J}_u. \tag{6}$$

where $p_j^u \in [0, 1]$ represents the proportion of relocation endpoints contributed by active operator j relative to all active operators in unit u.

We then define the Competition Index (CI) as the normalized Shannon entropy of these shares:

$$CI^u = -\frac{1}{\log M^u} \sum_{j \in \mathcal{J}_u} p_j^u \log p_j^u. \tag{7}$$

where the normalization term $1/\log M^u$ ensures the index is bounded in $[0, 1]$ for any $M^u \geq 2$, representing the degree of balance in relocation activities among active operators. By convention, if $M^u \leq 1$, we set $CI^u = 0$ as there is no inter-operator competition.

In units where only a single operator is active, competition is characterized by the intensity of exclusive operational intervention. We define the Exclusivity Index (EI) for operator j as:

$$EI_j^u = \begin{cases} n_j^u, & \text{if } M^u = 1 \text{ and } j \in \mathcal{J}_u, \\ 0, & \text{otherwise.} \end{cases} \tag{8}$$

where EI_j^u records the absolute number of relocation endpoints by operator j only when j is the sole active operator in the unit. EI is defined as a count to capture the intensity of exclusive intervention, which cannot be recovered from share-based measures under exclusivity. This metric is interpreted conditional on operator scale, as fleet size is controlled for in the model. The main variables and notation used in the spatiotemporal-unit analysis are summarized in Table 1.

Finally, the average idle energy consumption is modelled as a function of operational, spatial, and competitive factors through the following general formulation:

$$Y^u = f\left(\{F_j^u\}_j,\ D^{(z)},\ \text{POI}^{(z)},\ T^{(d)},\ W^{(d)},\ CI^u,\ \{EI_j^u\}_j\right) + \varepsilon^u. \tag{9}$$

Table 1
Summary of Variables for spatiotemporal unit u.

Symbol	Description
SOC_i^s, SOC_i^e	Battery state of charge at start and end of event i
F_j^u	Mean fleet size of operator j in unit u
$D^{(z)}$	Geodesic distance from region z centroid to city center
$POI^{(z)}$	Total number of POIs in region z (from Overpass API)
$T^{(d)}$	Mean air temperature on day d
$W^{(d)}$	Indicator equal to 1 for weekends or holidays, 0 otherwise
CI^u	Entropy-based indicator of inter-operator competition in unit u
EI_j^u	Exclusive relocations performed by operator j in unit u
Y^u	Mean idle energy consumption per idle event in unit u
N_{idle}^u	Number of idle events in unit u
n_j^u	Number of relocations into unit u by operator j
p_j^u	Share of relocations by operator j in unit u

where $f(\cdot)$ denotes the predictive function estimated in the modelling section, and ε^u is a zero-mean error term capturing unobserved influences. The inputs include operator-level fleet size $\{F_j^u\}_j$, spatial context $D^{(z)}$ and $POI^{(z)}$, day-level controls $T^{(d)}$ and $W^{(d)}$, and competition/exclusivity indicators CI^u and $\{EI_j^u\}_j$. This modelling framework enables a spatially detailed assessment of how idle energy consumption is shaped by local demand context, operator behaviors, and the competitive landscape between different service providers.

3.2. Interpretable Machine Learning Framework

3.2.1. Geographically-Aware Random Forest Regression

To systematically examine how operator competition indicators and spatial demand-supply conditions are associated with idle energy consumption in shared e-scooter systems, this study employs a geographically disaggregated machine learning framework based on random forest regression. As a tree-based ensemble method, random forest (RF) constructs an ensemble of decision trees using bootstrap samples of the training data and aggregates their predictions to form a robust estimator (Breiman, 2001). This technique is particularly well-suited to our context, as it accommodates non-linear, high-order interactions among explanatory variables and is robust to multicollinearity and noise–conditions commonly encountered in urban mobility data.

From a modelling perspective, random forest (RF) offers several advantages. First, it does not impose restrictive assumptions on the underlying data distribution or functional form. Second, it can capture spatial heterogeneity and local non-stationarity when combined with spatiotemporal structuring. Third, RF provides built-in mechanisms for estimating variable importance, facilitating post hoc interpretation of model behavior.

Let Y^u denote the average idle energy consumption per event observed in spatiotemporal unit u. Let $\mathbf{X}^u = \left(x_1^u, \ldots, x_p^u\right) \in \mathbb{R}^p$ denote the corresponding feature vector for unit u, where predictors include fleet size, POI density, distance to city center, temperature, weekend indicator, and indicators of operator competition and exclusivity.

The random forest model estimates the conditional expectation of Y^u given $\mathbf{X}^u$ as follows:

$$\hat{f}\left(\mathbf{X}^u\right) = \mathbb{E}\left[\, Y^u \mid \mathbf{X}^u \right] \approx \frac{1}{T} \sum_{t=1}^{T} f_t\left(\mathbf{X}^u\right), \tag{10}$$

where $f_t(\cdot)$ is the prediction of the t-th decision tree, and T denotes the total number of trees. Each tree f_t is trained on a bootstrap sample drawn with replacement and constructed via recursive binary splitting to minimise the mean squared error (MSE) at each node. At each split, a random subset of features is evaluated to promote diversity among trees and mitigate overfitting.

3.2.2. Model Interpretation with SHAP Values

While random forest models typically exhibit strong predictive performance, their ensemble structure often limits direct interpretability. To address this limitation, we employ SHAP (SHapley Additive exPlanations) (Lundberg and Lee, 2017), a theoretically grounded method derived from cooperative game theory that attributes a prediction to individual input features. SHAP assigns each feature a contribution score representing its marginal contribution to the model's prediction (Molnar, 2020).

Given a prediction $\hat{f}\left(\mathbf{X}^u\right)$, the SHAP framework decomposes it as:

$$\hat{f}\left(\mathbf{X}^u\right) = \phi_0 + \sum_{j=1}^{p} \phi_j^u, \tag{11}$$

where $\phi_0 = \mathbb{E}[Y]$ denotes the model's expected output (the baseline prediction), and ϕ_j^u represents the SHAP value for the j-th feature in unit u, reflecting its marginal contribution to the predicted outcome. These values are computed by averaging the marginal contributions of each feature across all possible subsets of the predictor variables, ensuring fair and consistent attribution.

SHAP values are used here for model interpretation rather than causal identification. They quantify how each feature contributes to the prediction of a fitted random-forest model, conditional on the observed covariates included in the model. Therefore, positive or negative SHAP contributions should be interpreted as descriptive within-model associations with predicted idle energy consumption, not as causal effects.

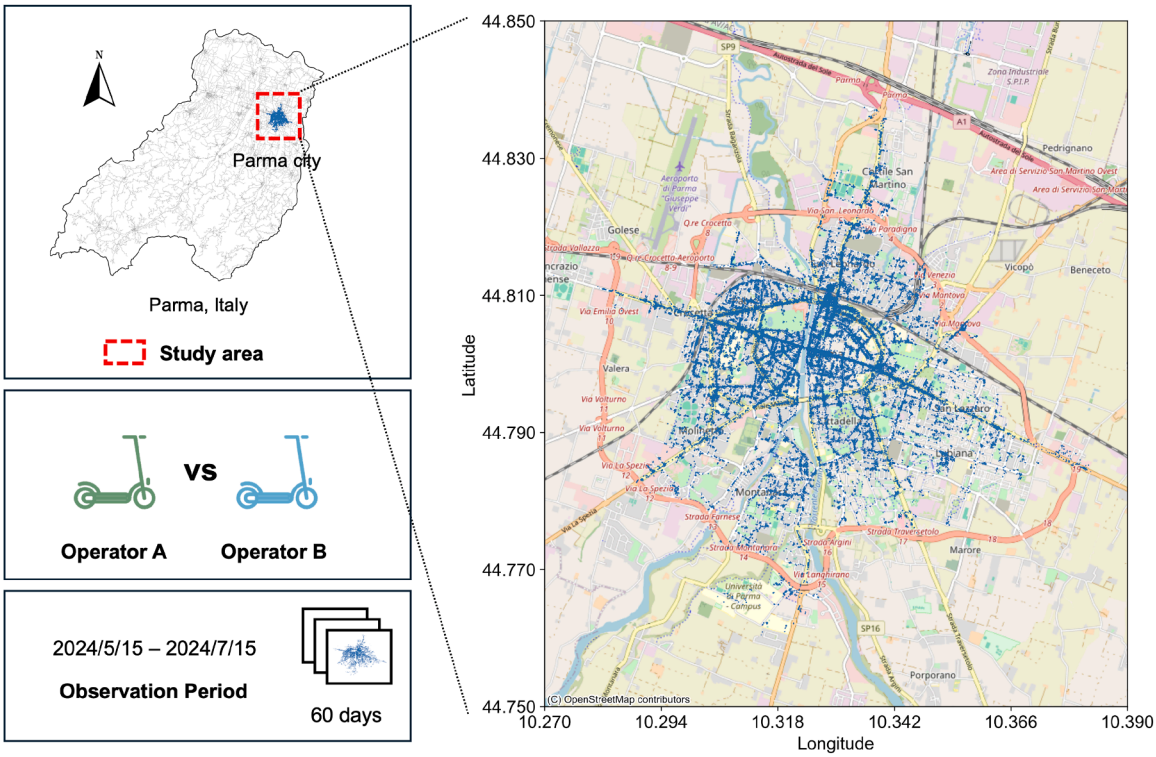

Fig. 2. Overview of Study area, Period, and E-scooter Operators.

In our empirical analysis, SHAP values are employed to identify the most influential predictors of idle energy consumption, enabling a systematic evaluation of feature importance. Specifically, we examine how competition intensity and fleet size are associated with the model's predictions on energy waste, examining whether higher values of these variables correspond to increased inefficiencies. Moreover, the spatial variation in these relationships is analyzed to generate insights that inform operator-level deployment strategies and urban policy interventions.

In summary, the geographically structured RF model and SHAP-based interpretation constitute a robust analytical pipeline that aligns with the data's spatial resolution and supports interpretable, high-fidelity prediction and model-based interpretation. This methodology is particularly effective in revealing the operational mechanisms and inefficiencies associated with multi-operator competition in shared micromobility systems.

4. Empirical Study

This section presents an empirical study of shared e-scooter operations in Parma, where two operators coexisted over the studied period. We detail the data processing steps used to reconstruct e-scooter lifecycle events, calibrate energy consumption measures across operators, and derive spatially resolved indicators of competition and energy consumption. By examining real-world operational dynamics, this study provides critical evidence to validate our modeling approach and reveals how competitive behavior manifests in urban contexts, thereby demonstrating the practical relevance and feasibility of our analytical framework.

4.1. Study Area

Parma is a city with active shared e-scooter operations, where multiple operators have entered and exited the market since its initial adoption. The composition of operators remains dynamic, and their operational strategies evolve frequently. We analyze operational data from a period when two operators, namely Operator A and Operator B, were simultaneously active in Parma. Fig. 2 illustrates the scope of this paper. The data span from 15 May 2024 to 13 July 2024, during which Operator A and Operator B were the only two companies providing e-scooter services in the city.

4.2. Data Preparation

4.2.1. Data description

The raw dataset consists of snapshots of all idle e-scooters in the city, taken every three minutes. Each snapshot includes the e-scooter's timestamp, geographic coordinates, battery level, and unique identifier. Fig. 3(a) displays the total number of distinct

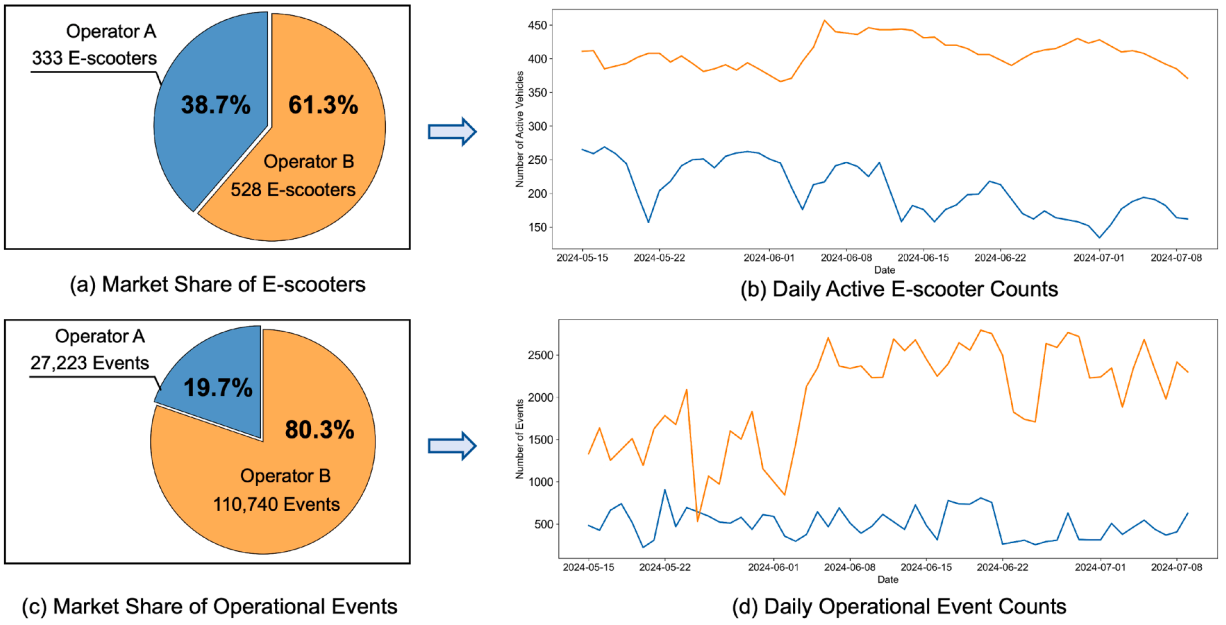

Fig. 3. Fleet Size and Operational Event Share Reflecting Operator Imbalance.

vehicle identifiers recorded for each operator, representing their respective fleet sizes. Operator A deployed 333 scooters, accounting for 38.7%, while Operator B deployed 528 scooters, making up 61.3%. Fig. 3(b) illustrates the day-by-day variation in fleet size. Operator B maintained a consistently larger presence. Fluctuations in fleet size suggest a pattern of coordinated shifts between the two operators. Fig. 3(c) and Fig. 3(d) illustrate the market share of operational events and their daily counts. Overall, Operator A accounted for 19.7% of events, while Operator B contributed 80.3%, indicating an even more pronounced imbalance than reflected in the fleet sizes. We refer to Operator B as the dominant operator and Operator A as the nondominant operator. In summary, the statistical analysis confirms that two operators coexisted in Parma with a significant disparity in both fleet size and operational volume during the study period.

As described earlier in Section 3.1, the lifecycle of each e-scooter was reconstructed as a time-ordered sequence of operational records, and each operational segment was treated as an event. For each event, we calculated distance using the Haversine formula (Inman, 1849), duration, SOC change, and SOC loss per kilometer. The event labels were then assigned using a rule-based procedure based on observable physical signatures in the data. This type of rule-based preprocessing is commonly used in empirical shared-mobility studies when trips or operational states have to be inferred from vehicle records using time, distance, and energy-related filters (Heumann et al., 2021; Caspi et al., 2020). In our case, the rules were developed by manually inspecting continuous scooter histories and by examining the empirical distributions of transition distance, SOC change, and SOC loss per kilometer. These diagnostics showed recurring patterns that are consistent with the operational meanings of the event types: gradual positive SOC changes during station charging, abrupt large SOC increases during battery replacement, non-trivial movement with SOC loss during rides, longer zero-SOC movements during relocation, and short-distance non-increasing-SOC intervals during idle periods.

We define ΔSOC as end SOC minus start SOC. A positive ΔSOC was treated as a charging or battery-replenishment signature and was therefore not allowed to enter the idle class. Small positive SOC increases were labelled as station charging, whereas abrupt increases of at least 20 percentage points were labelled as battery swaps. For records without SOC increase, short-distance intervals were treated as idle, while longer zero-SOC movements over consecutive records were treated as relocation. Ride events required non-trivial movement, SOC loss, and SOC loss per kilometer within the normal riding range; abnormal high SOC-loss-per-kilometer observations were excluded from ride classification. The thresholds in Table 2 are not intended to be unique statistical cutoffs. Rather, they are conservative empirical-operational boundaries used to separate physically different lifecycle states. Since the main

Table 2
Criteria for labeling operational states.

Condition	Assigned label
Duration $\geq$ 24 hours	Deactivation
ΔSOC $\geq$ 20	Battery swap
$0 < \Delta$SOC < 20	Station charging
Distance $\geq$ 20 m, ΔSOC = 0, and three or more consecutive records	Relocation
Distance $\geq$ 20 m, ΔSOC < 0, and SOC loss/km in $(0, 20]$	Ride
Distance < 20 m and ΔSOC ≤ 0	Idle
SOC loss/km > 20 or physically inconsistent records	Excluded as abnormal records

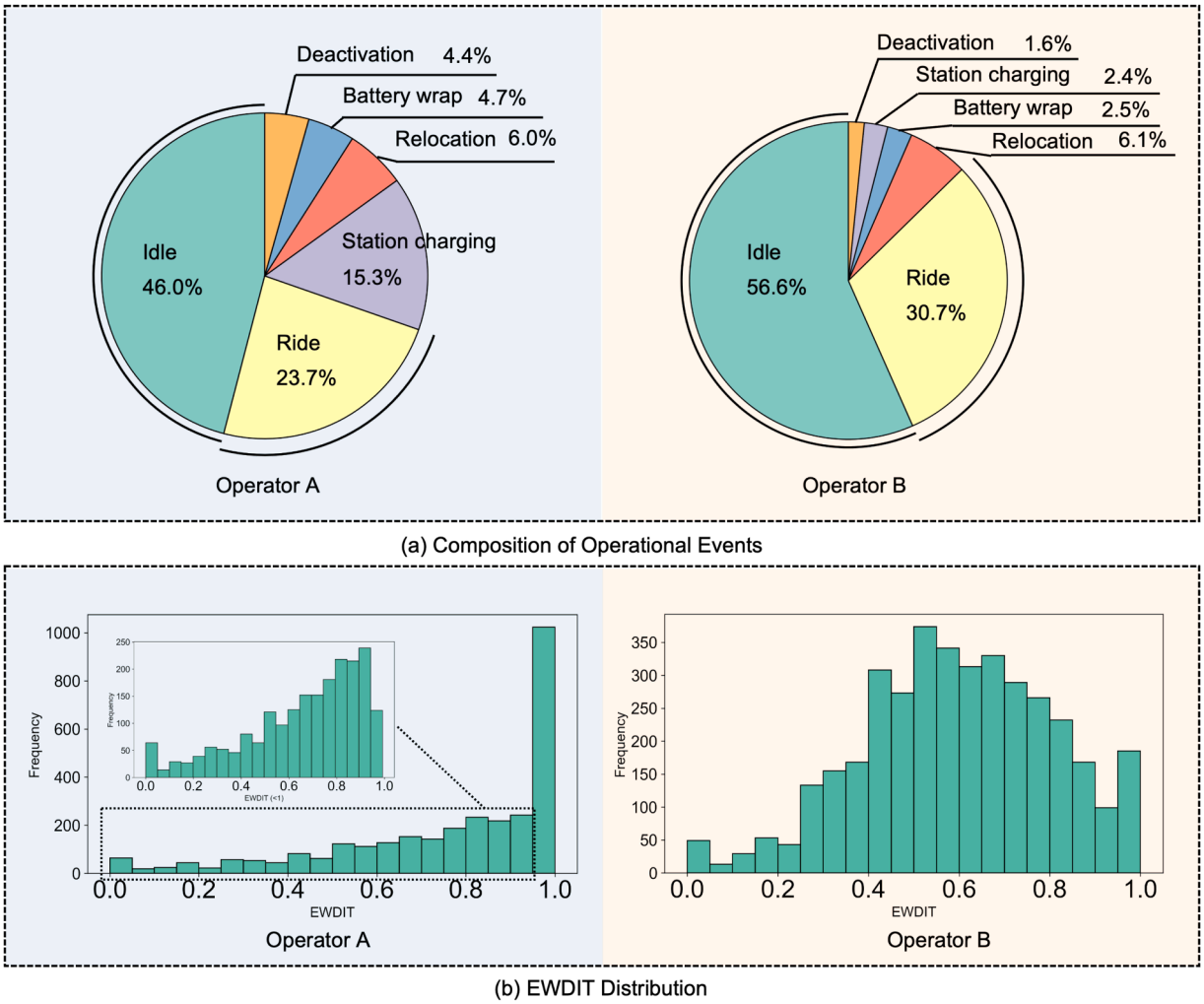

Fig. 4. Idle-State Proportion and Its Contribution to Energy Consumption.

outcome of this study is idle energy consumption, the key requirement is that the Idle class is not materially mixed with charging, battery-swapping, relocation, or ride periods. The Idle class was overwhelmingly short-distance and discharging: the median recorded displacement was 3.55 m and the 95th percentile was 14.46 m, both below the 20 m stationary boundary, and the median SOC loss was 2.00 percentage points. No battery-swap-like SOC-increase signature appeared in the Idle class. The Ride class also showed the expected non-stationary and SOC-losing pattern, with a median recorded displacement of 1,283.56 m and a median SOC loss of 4.00 percentage points. Consecutive records with identical state labels may arise due to the logging mechanism, particularly during relocation. To avoid fragmenting a single operational activity into multiple events, sequences of three or more consecutive records with the same state were merged, and the duration, distance, and SOC difference were recalculated for the merged interval.

Following these steps, we obtained clearly labeled lifecycle datasets for both operators. The proportions of events by operational state are shown in Fig. 4(a). As illustrated, idle events account for the largest share, comprising nearly half of all records, followed by ride events. The large number of idle events is expected, as transitions between operational states always pass through an idle state. As a result, idle events naturally constitute a majority.

Ride events represent the actual mobility services that operators aim to deliver. However, they account for only 20% to 30% of all operational events, underscoring a pronounced mismatch between actual rides and operational expectations. To evaluate electricity consumption during idle periods, we employ an indicator known as Electricity Wasted During Idle Time (EWDIT) (Li et al., 2022). This metric quantifies the proportion of total discharged energy that is consumed during idle states within a single discharging cycle. The calculation relies on changes in the state of charge (SOC) and is defined as follows:

$$\mathrm{EWDIT} = 1 - \frac{\sum_{i \in DC} \left(\mathrm{SOC}_i^s - \mathrm{SOC}_i^e\right)}{\mathrm{SOC}_{DC}^s - \mathrm{SOC}_{DC}^e}. \tag{12}$$

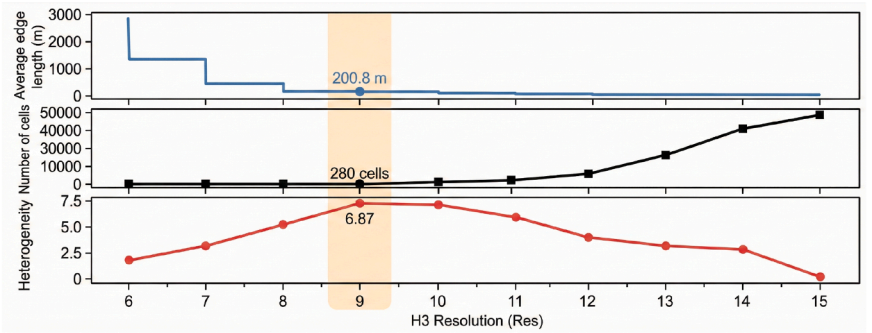

(a) H3 Hexagon Cell Metrics and Regional Heterogeneity

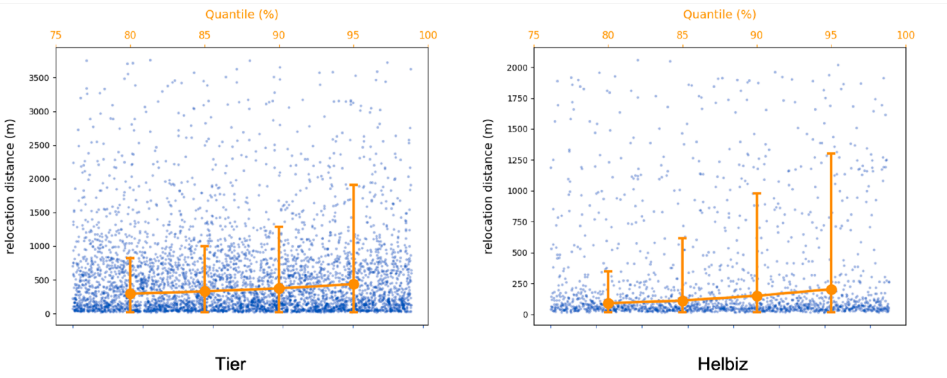

(b) Relocation Distance Scatter Plot with Statistical

Fig. 5. Rationale for Choosing H3 Resolution.

where DC denotes a single discharging cycle, and i indexes the i-th ride event within that cycle. The variables SOC^{s}_{DC} and SOC^{e}_{DC} represent the battery state of charge at the start and end of the discharging cycle, respectively, while SOC^{s}_{i} and SOC^{e}_{i} denote the battery SOC at the start and end of the i-th ride event.

Fig. 4(b) illustrates the frequency distribution of EWDIT values, highlighting substantial idle-state energy wastage for one operator, particularly when no rides occur between charging events. For the other operator, EWDIT values frequently range between 0.5 and 0.8, indicating considerable idle energy consumption.

4.2.2. H3 Resolution Determination

To obtain region-day data, the precision of the H3 indexing method must first be determined. The H3 method partitions space into hexagonal grids, with resolution controlling the size and number of these grids. As shown in Fig. 5(a), the blue line indicates the average edge length of hexagonal grids at different H3 resolutions. The red line illustrates the heterogeneity of the competition index across resolutions, measured using Shannon entropy. The black line shows the total number of H3 cells that cover all event start points of both operators within the study area.

As shown in Fig. 5(b), the relocation distances of both operators are mainly concentrated around 250 meters. At H3 resolution 9, the average edge length of each hexagonal cell is about 200 meters. This implies that the distance between the centers of adjacent cells is approximately consistent with the observed relocation distances.

At this resolution, the competition index exhibits close-to-maximum heterogeneity, which effectively reflects the spatial variation in competitive intensity. The number of cells at this level also remains within a reasonable range, avoiding excessive computational burden in geographic analysis. Resolution 9 therefore represents a balanced choice between capturing relocation distance characteristics, maintaining computational feasibility, and preserving spatial heterogeneity. Sensitivity checks using adjacent resolutions (8 and 10) produced qualitatively similar spatial patterns and model outcomes, confirming that the results are robust to reasonable variations in grid resolution.

4.2.3. Energy Consumption Calibration Across Operators

Given that scooter models and BMS calibration may differ across operators, SOC is a BMS-reported proxy and the mapping between physical energy and SOC can be operator-specific. Since the purpose of this paper is to analyze operational behavior under multi-operator coexistence rather than to compare scooter engineering quality, we calibrate the SOC-based proxy to reduce the risk that cross-operator contrasts are dominated by systematic SOC scale differences. To anchor the calibration in an operationally interpretable context, we use ride events and compute depletion rates (%/km) as the absolute SOC change divided by ride distance.

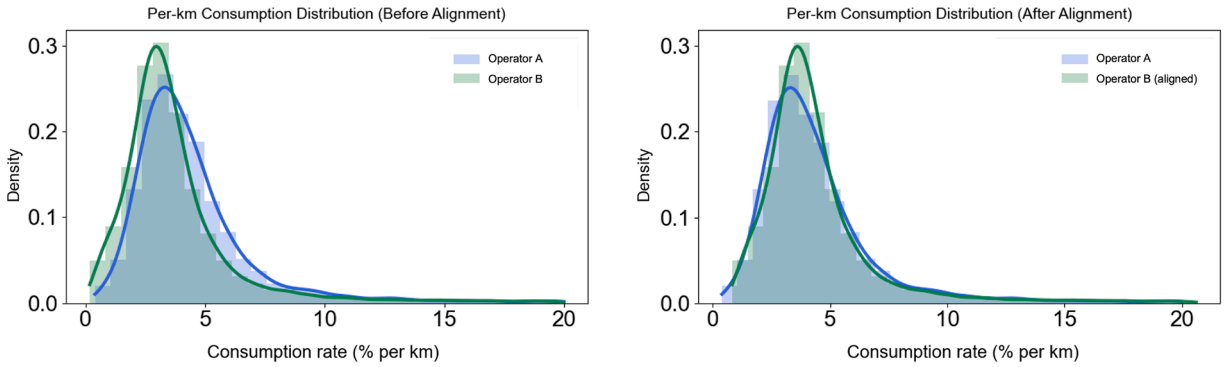

Fig. 6. Comparison of Battery Data Distributions Before and After Calibration.

Specifically, consumption rates (%/km) from all "Ride" events were extracted and statistically compared between Operator A (n = 6,273) and Operator B (n = 30,938). Initial statistical analyses indicated significant differences in means, standard deviations, medians, and overall distributions between the two datasets. Kolmogorov–Smirnov (KS) tests, Welch's t-tests, Mann–Whitney U-tests, and Levene's tests all confirmed significant statistical differences ($p < 0.001$), with Cohen's d equal to 0.253, suggesting a moderate effect size. Therefore, a mean–standard-deviation alignment was performed to rescale Operator B's ride-event depletion rates onto Operator A's SOC-equivalent scale:

$$r_{\text{Operator B, aligned}} = \left(r_{\text{Operator B}} - \bar{r}_{\text{Operator B}}\right) \cdot \frac{\sigma_{\text{Operator A}}}{\sigma_{\text{Operator B}}} + \bar{r}_{\text{Operator A}}. \tag{13}$$

This alignment is an affine rescaling that preserves within-operator heterogeneity (i.e., the relative ordering of depletion rates within Operator B) while harmonizing the scale of the SOC-based proxy across operators. It does not imply that scooter technologies are identical; rather, it supports operational comparisons under a common SOC-equivalent scale, reducing the likelihood that subsequent analyses confound operational patterns with BMS scale differences.

Fig. 6 illustrates the distribution of ride-event depletion rates before and after calibration for both operators. Post-alignment analyses revealed identical means (4.407) and standard deviations (2.580) for the aligned Operator B series and the Operator A series. Statistical tests after alignment showed no significant differences in means (t-test, $p = 1.000$) or medians (Mann–Whitney U-test, $p = 0.2197$), and Cohen's d approached zero, indicating successful alignment in central tendency and dispersion on the SOC-equivalent scale. However, minor yet statistically significant differences remained in higher-order distribution characteristics (KS test, $p < 0.001$; Levene's test, $p < 0.001$). We retain these residual distributional differences to preserve the empirical shape of each operator's data, and we avoid interpreting the alignment as removing genuine technological differences.

The alignment affects the SOC scale for Operator B only, while leaving Operator A unchanged. Accordingly, the strongest competition-related patterns emphasized in this study for the nondominant operator are not altered by this preprocessing choice. We interpret cross-operator comparisons as operational contrasts under a harmonized SOC-equivalent scale, rather than as differences in scooter engineering quality. As a robustness check, we repeated the main analysis without applying the alignment, and the key competition-related patterns and conclusions remained qualitatively unchanged. Subsequently, idle energy consumption was recalculated based on the calibrated SOC-equivalent series.

4.3. Results

4.3.1. Variable Construction

The spatial distribution of predictors (features) and outcomes (targets) is shown in Fig. 7. Each day is represented as a snapshot covering all spatial units. We visualize the average values over the 60-day period to provide an intuitive representation. To enhance the interpretability of these heatmaps, specific data processing steps were applied to different variables. For the competition index, values were capped at 0.5 and discretized into 50 bins of width 0.01. Fleet size and POI density maps were clipped at the 5th and 95th percentiles and linearly scaled. Exclusivity indices were categorized using quantile-based binning at 0%, 50%, 75%, 90%, 95%, and 100% percentiles.

First, among the five maps related to competition variables (shown with a blue base color), both the competition index and fleet sizes exhibit higher intensity in the city center, while competition diminishes noticeably toward peripheral areas. Operator B generally deploys a larger fleet than Operator A, with certain peripheral zones primarily serviced and operated by Operator B. Regarding the exclusivity index maps, although Operator B demonstrates overall stronger exclusivity, the two operators display distinct spatial patterns. Operator A's high-exclusivity areas are more dispersed across the urban area, whereas Operator B's exclusivity is more concentrated in the city center. This suggests that some central zones are dominated by the leading operator, while the less dominant operator finds opportunities to establish exclusive markets in more scattered peripheral regions.

With respect to the dependent variable (mean idle energy consumption per idle event), the overall map indicates lower per-idle consumption in central areas compared to peripheral regions. This pattern describes a per-event micro-scale outcome and should not

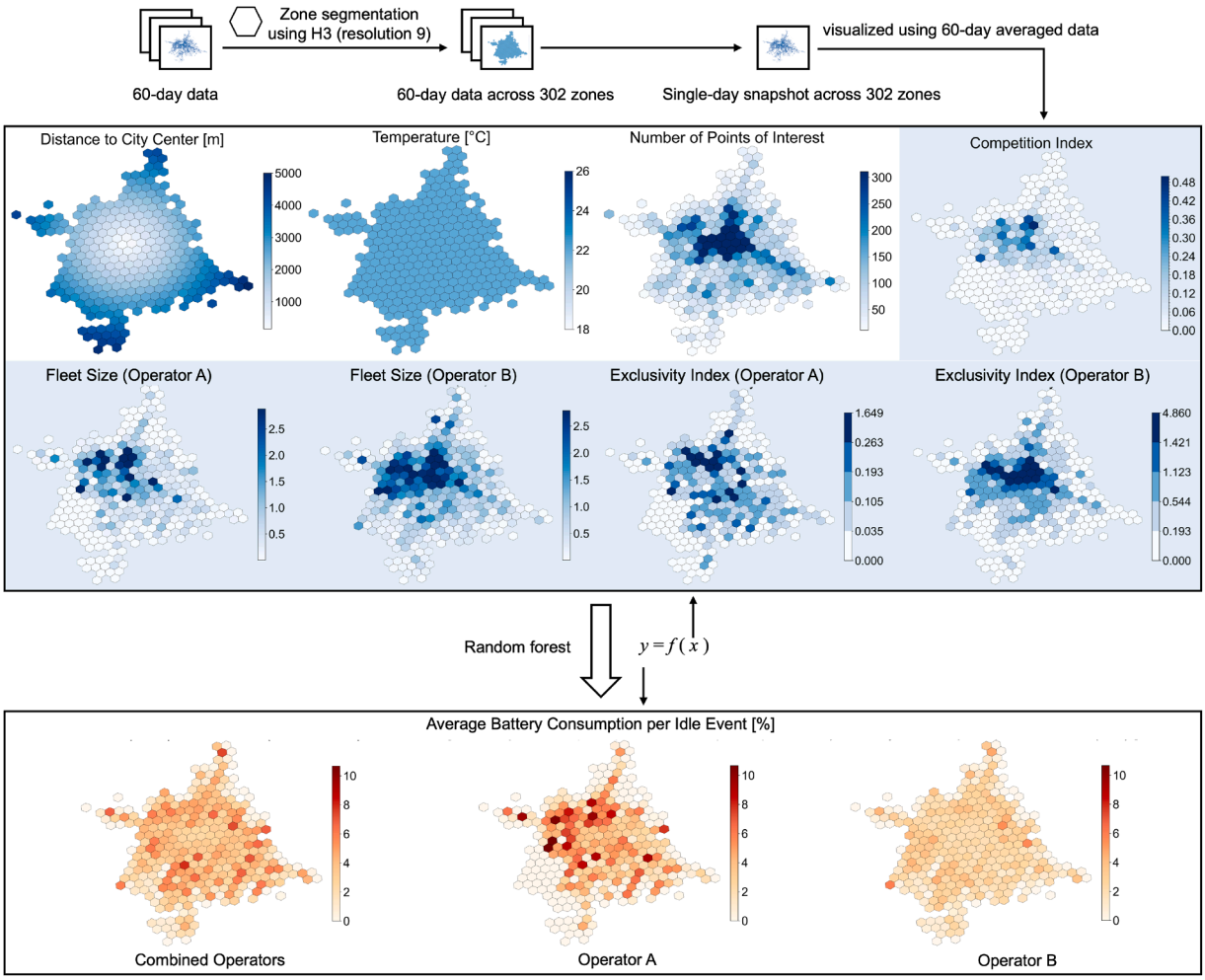

Fig. 7. Spatial Overview of Explanatory and Dependent Variables.

be read as the unit-level total idle energy burden, which also depends on exposure such as the frequency and duration of idle spells. To provide exposure context, we also examine N^{u}_{idle}, the number of idle events in each cell–day. N^{u}_{idle} varies substantially across space and time, reflecting differences in local demand intensity and deployment scale. Therefore, a cell–day with a moderate per-idle value can still generate a large total idle loss when idle exposure is high, while a cell–day with a high per-idle value can contribute less to total burden when idle events are rare. The per-idle maps are interpreted together with this exposure context. This pattern aligns with higher vehicle turnover in zones characterized by dense user activity. In the operator-specific maps, Operator A displays considerable spatial variability, with several areas exhibiting notably high idle energy consumption. In contrast, Operator B maintains consistently lower and more uniform idle consumption across different regions. These findings suggest that, as the dominant operator, Operator B operates in a more efficient and sustainable manner.

4.3.2. Feature Contributions to Idle Energy Consumption

To ground SHAP-based interpretation in predictive generalization, we report out-of-sample predictive performance for the Random Forest models. We evaluate the overall model and the operator-specific models on a held-out test set (75/25 split, holding out the later portion of the study window) and report test-set R^2, RMSE, and MAE. Error metrics are expressed in SOC percentage points. Table 3 summarizes the test-set performance:

In this subsection, we examine how different factors contribute to idle energy consumption using SHAP. In all SHAP plots, the x-axis shows the feature value and the y-axis shows the SHAP contribution in SOC percentage points, which indicates how the feature shifts the predicted idle energy consumption relative to the model baseline. Positive SHAP values indicate higher predicted idle energy consumption and negative values indicate lower predictions; larger absolute values indicate stronger contributions. When a color scale is shown, it encodes the interacting feature.

Fig. 8(a) reports the pooled (two-operator) model, while Fig. 8(b) and Fig. 8(c) report the operator-specific models for Operator A and Operator B, respectively. In each panel, the left plot is a SHAP summary (beeswarm) plot where each point represents a cell–day

Table 3
Test-set predictive performance of Random Forest models.

Model	Test-set R^2	Test-set RMSE	Test-set MAE
Overall (all operators)	0.134	2.973	2.007
Operator A (non-dominant)	0.099	2.526	1.621
Operator B (dominant)	0.082	8.567	5.606

observation; the horizontal position is the SHAP contribution and the color indicates the feature value (low to high). The right plot shows feature-importance proportions based on normalized mean absolute SHAP values, which summarize within-model contribution to prediction rather than variance explained.

For the Competition Index dependence plots in Fig. 9, each point corresponds to a cell–day observation; the fitted curve summarizes the average dependence pattern and the shaded band indicates uncertainty. Vertical thresholds and background shading indicate the competition regimes used in the text. For the interaction plot in Fig. 10, the color bar encodes distance to center, illustrating how the competition association varies across spatial context. Each figure combines two views: on the left, the SHAP value summary plot ranks features by their contribution to predictions. On the right, the corresponding share of total importance is shown. The analysis focuses on strategic competition, represented by fleet size (baseline deployment) and the competition index (relocation-based rivalry). Together with exclusivity measures, these competition-related indicators account for a large share of within-model importance as measured by aggregated absolute SHAP values (66.6% in the overall model, 70.0% for Operator A, and 71.8% for Operator B). We define competition-related predictors as the fleet size variable(s), the normalized Competition Index constructed from relocation shares, and the operator-specific Exclusivity Index variables. The reported percentage is computed as a SHAP-based within-model importance share. For each feature j, we compute its mean absolute SHAP value over the evaluation sample, $I_j = \frac{1}{|S|}\sum_{u\in S}|\phi_j^u|$, and we normalize by the total across all features to obtain an importance share $I_j / \sum_h I_h$; the competition-related percentage is the sum of importance shares over this feature set. The reported values correspond to sums of the plotted SHAP importance shares: 66.6% = 36.9% + 28.2% + 1.5%, 70.0% = 59.8% + 1.8% + 8.4%, and 71.8% = 70.4% + 1.1% + 0.3%. It is important to clarify that this quantity refers to the share of feature attribution within the model, rather than variance explained out-of-sample (variance explained is evaluated using test-set R^2, as reported in Table 3).

In Fig. 8(a), the SHAP summary plot indicates that the two most influential factors are the fleet sizes of Operator A and Operator B, contributing 36.9% and 28.2% of the total importance, respectively. On the side where average idle energy consumption is reduced (i.e., negative SHAP values), the corresponding observations are associated with smaller fleet sizes (blue points). There are no data points indicating that larger fleet sizes help reduce idle energy consumption. This pattern is consistent with the interpretation that larger fleet sizes may reflect oversupply in some spatiotemporal units, which co-occurs with higher idle energy consumption. On the side where idle energy consumption is promoted (i.e., positive SHAP values), both larger (red) and smaller (blue) fleet sizes appear. This implies that a larger fleet size does not consistently lead to higher energy waste–some areas with high deployment do show waste, while others with small fleets still experience high idle energy consumption.

The exclusivity index for Operator A is identified as the third most important variable in the model, while Operator B's exclusivity index ranks the lowest. A higher exclusivity index for Operator A is associated with an increase in average idle energy consumption. This suggests that when Operator A is the sole operator in a given area, its deployments often lead to greater energy waste. In contrast, Operator B's exclusive presence shows minimal influence on idle energy use. These results imply that Operator A's relocation strategies may be less effective in matching supply with local demand, compared to those of Operator B.

Other variables, ranked by importance, include distance to city center, temperature, number of POIs, and the weekend indicator. Being farther from the city center and having fewer POIs are both associated with higher average idle energy consumption. Lower temperatures also lead to higher consumption, possibly due to both reduced riding demand and faster battery depletion. The weekend indicator slightly increases average idle energy consumption, but its influence is minor and the pattern is not clearly defined.

By comparing Fig. 8(b) and Fig. 8(c), the SHAP value axis shows that the Operator A model exhibits larger absolute SHAP values. This indicates that, overall, Operator A (the weaker operator) is more sensitive to the independent variables than Operator B (the stronger operator). Regarding the competitive index, its importance is significantly higher in the Operator A model (ranked third), while in the Operator B model, this variable has negligible impact. This indicates that the association between relocation-based competition and predicted idle energy consumption is stronger for the nondominant operator, while it is weaker for the dominant operator in our fitted model.

4.3.3. Univariate Association Analysis of Competition-Related Factors

Among the various drivers of idle energy consumption, operator competition warrants particular attention. Fleet size reflects a relatively stable, baseline deployment strategy, whereas relocation actions are more flexible and proactive choices that directly shape market rivalry. To capture these dynamics, we use the competition index as a key measure of relocation-based competition. This subsection examines its univariate association on average idle energy consumption, providing a more focused view of how competition intensity translates into operational inefficiency.

As shown in Fig. 9(a-c), the relationship between the competition index and SHAP values exhibits a similar pattern across the Operator A model, total model, and Operator B model. When the competition index is zero or low, the SHAP values for the competition index tend to be negative, indicating lower predicted idle energy consumption relative to the model baseline. As the competition index increases, the SHAP values become positive on average, indicating an association between higher competition intensity and higher

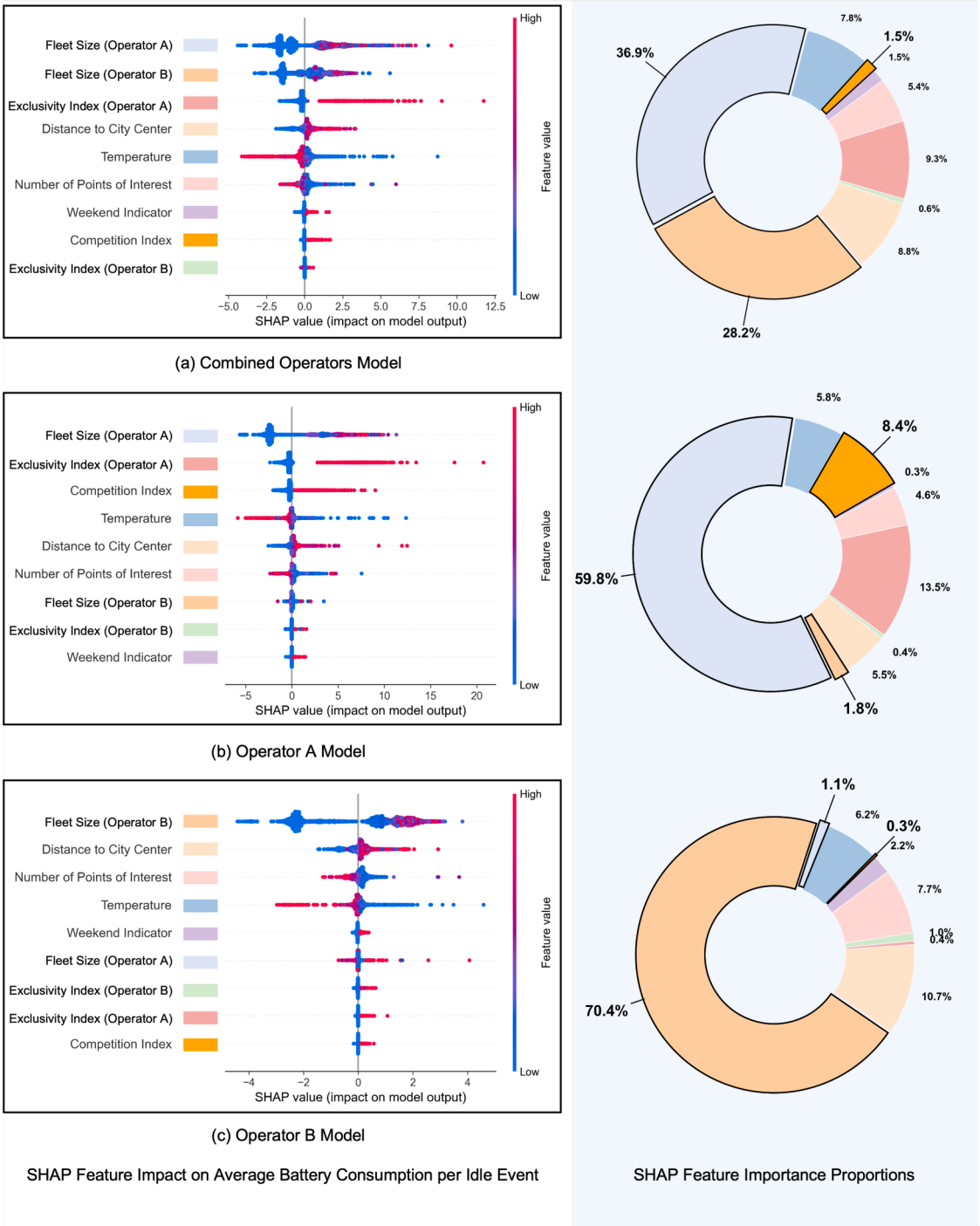

Fig. 8. Summary of SHAP values and feature contributions.

Notes: The left panel is a SHAP summary plot (points are cell–day observations; color indicates feature value). The right panel reports feature-importance proportions based on normalized mean absolute SHAP values.

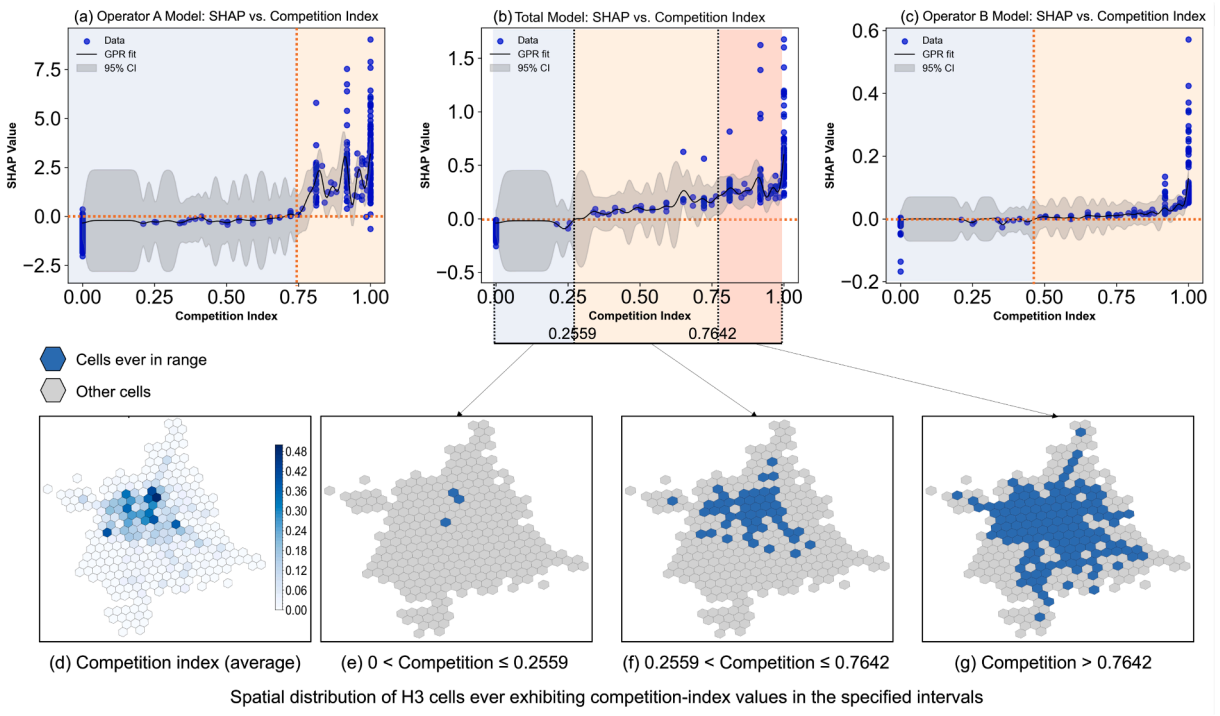

Fig. 9. SHAP-based dependence of the Competition Index and its spatial distribution.
Notes: Points are cell–day observations; the curve summarizes the average dependence and the shaded band indicates uncertainty. Vertical thresholds and background shading indicate the competition regimes used in the text.

predicted idle energy consumption. These patterns indicate that higher competition intensity is associated with higher predicted idle energy consumption in the fitted model; we refer to the high-intensity regime as “harmful competition” in terms of operational efficiency.

To illustrate this trend in more detail, we take the total model (Fig. 9(b)) as an example. A Gaussian regression was applied to the data points, showing a nonlinear relationship between the competition index and SHAP values. To classify the competition index, we used the Jenks Natural Breaks method to identify two threshold values. This method minimizes variance within groups and maximizes variance between them, effectively detecting natural divisions in the data. Including the case where the competition index is zero, we define four categories: (1) no competition (competition index = 0), (2) minor competition (0-0.2559), (3) mild competition (0.2559-0.7642), and (4) harmful competition (>0.7642).

Each data point corresponds to a specific area on a specific day. The spatial distribution of the three competition categories over the 60-day study period is shown in Fig. 9(e-g). An area is marked if any data point within that area falls into a given category during the study period. Fig. 9(d) presents the average competition index across the 60-day period, revealing that competition intensity remains highest in central urban areas and gradually diminishes toward the periphery. Fig. 9(e) highlights only three areas that experienced benign competition, confirming that this condition is rare. Fig. 9(f) shows regions where mild competition occurred, while Fig. 9(g) identifies areas with harmful competition. Notably, an unexpected yet critical observation is that benign competition zones are extremely limited, whereas areas experiencing harmful competition are the most prevalent. This finding suggests a market dynamic where competitive behaviors tend to escalate into harmful intensity rather than stabilizing at moderate, mutually beneficial levels, which raises concerns from both operational efficiency and sustainability perspectives. Overall, apart from the no-competition case, harmful competition is the most common category, followed by mild competition. Benign competition appears in only a few locations.

Comparing the Operator A model (Fig. 9(a)) with the Operator B model (Fig. 9(c)), we observe that the Operator A model shows a clearer and stronger pattern. SHAP values in this model vary more substantially with the competition index. In contrast, most SHAP values in the Operator B model remain close to zero. Only at very high competition-index values do we observe noticeably positive SHAP contributions for Operator B, suggesting a weaker association for the dominant operator. This indicates that the weaker operator, Operator A, is more sensitive to competition. As a result, Operator A may need to reconsider aggressive relocation strategies and avoid over-deployment in competitive areas to improve energy efficiency and operational outcomes.

To assess whether the Competition Index pattern depends on the original demand-proxy choices, we conducted a robustness check using alternative demand controls. In addition to the original specification with POI density and distance to the city center, we estimated three alternative specifications: one adding public-transport accessibility controls, one adding WorldPop population density, and one replacing the original POI and distance-to-center controls with population density and transit-accessibility controls. This check

Table 4
Robustness of the Competition Index pattern to alternative demand-proxy specifications.

Model	Original	+ Transit	+ Population	Population + transit
Combined	0.807	0.792	0.806	0.544
Operator A	2.884	2.908	2.859	2.982
Operator B	0.246	0.245	0.242	0.174

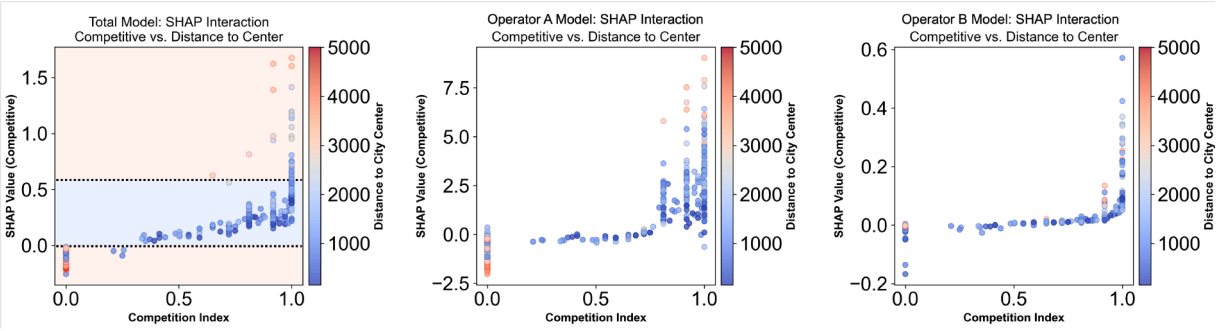

Fig. 10. SHAP interaction between Competition Index and distance to center.
Notes: Points are cell–day observations; color encodes distance to center.

is intended to evaluate the directional stability of the Competition Index pattern under alternative demand-proxy definitions, rather than to replace the main model-validation results reported above. We used the same competition-regime thresholds as in the SHAP dependence analysis: low-CI observations are those with $CI \leq 0.2559$, and high-CI observations are those with $CI > 0.7642$. For each refitted model, we computed the mean SHAP contribution of the Competition Index in the high-CI group minus that in the low-CI group. As shown in Table 4, this difference remained positive in the combined model and in both operator-specific models across all specifications. These results suggest that the descriptive Competition Index pattern is not driven by a single demand-proxy definition.

4.3.4. Bivariate Association Analysis of Competition-Related Factors

In addition to the direct association, competition also interacts with other variables. One notable interaction is with the variable distance to center. As shown in Fig. 10, data points with large distance to center values are mainly located at the top and bottom of the plot. In contrast, small distance values are concentrated around points with SHAP values close to zero. This pattern indicates that the association between competition and predicted idle energy consumption is stronger in suburban areas than in central urban areas.

A second interaction arises with fleet size. When fleet size is small, the association between competition and predicted idle energy consumption is more noticeable. When fleet size is large, this association is weaker. This finding is intuitive, because vehicle turnover is high in dense city centers, and thus the system is more resilient to variations in deployment. In contrast, on the urban periphery, competition interacts strongly with supply imbalances, leading to greater inefficiency.

These insights highlight the asymmetric risks of competition. The weaker operator, already more vulnerable to rivalry, should avoid relocation strategies driven purely by competitive motives. More broadly, operators must exercise particular caution when reallocating vehicles in peripheral areas, where competition-related inefficiencies are most pronounced.

5. Discussion

This section draws on the empirical findings to extract insights into the interplay between inter-operator competition and operational efficiency in shared e-scooter systems. We highlight the ways competitive dynamics are associated with spatial heterogeneity in idle energy consumption, reveal the particular vulnerabilities of weaker operators under intense competition, and outline strategies that could mitigate these inefficiencies. By linking quantitative evidence to practical recommendations, the discussion bridges analytical insights with policy and operational decision-making, advancing both academic understanding and the pursuit of sustainable urban mobility.

5.1. Insights into Competitive Dynamics and Operational Efficiency

A key finding of this study is the pronounced spatial heterogeneity in both competitive dynamics and operational efficiency among e-scooter operators. The concentration of higher competition indices and larger fleet sizes in central urban areas, contrasted with their significant reduction toward peripheral zones, suggests a spatially polarized market structure. Operator B, as the dominant actor, maintains larger and more uniformly distributed fleets, including in some peripheral zones where Operator A has minimal presence.

This asymmetric deployment indicates a strategic advantage for Operator B in consolidating market dominance, particularly in central regions.

The results also indicate that operator-specific exclusivity patterns are not merely reflections of market share but are spatially structured phenomena. Operator A's high-exclusivity zones are scattered and fragmented, while Operator B's exclusivity is tightly clustered in urban cores. Such a distribution suggests that market dominance in central areas is achieved at the expense of spatial fragmentation for less dominant operators, who must seek niche exclusivity in peripheral locations. This fragmentation is accompanied by higher variability in idle energy consumption for Operator A.

The relationship between fleet size and idle energy consumption underscores a critical operational trade-off. Larger fleet sizes, while intuitively expected to match higher demand, are not unequivocally associated with improved energy efficiency. Instead, the results indicate diminishing returns and potential oversupply, as both large and small fleets can correlate with elevated idle energy usage. This finding implies that beyond a certain threshold, additional fleet expansion may exacerbate idle losses rather than mitigate them, highlighting the necessity for precise demand-supply calibration in fleet management. We interpret competition through two complementary operational channels. Fleet deployment reflects a scale-based competitive stance and accounts for a large share of within-model importance, particularly for the dominant operator. The relocation-based Competition Index captures dynamic operational rivalry and is most informative for explaining heterogeneity for the non-dominant operator and in peripheral or lower-activity contexts. We therefore present relocation-based competition as a context-sensitive correlate rather than a universally dominant driver.

Insights from the competition index demonstrate that competitive pressure, especially in the form of aggressive relocation strategies, shows a non-linear association on idle energy consumption. Low or absent competition is generally associated with lower idle energy use, whereas higher competition intensity is associated with higher predicted idle energy consumption. This effect is notably more pronounced for the weaker operator, Operator A, whose idle energy consumption exhibits greater sensitivity to rising competitive intensity. This asymmetry suggests that competition-driven relocations co-occur with higher predicted idle energy consumption for the nondominant operator, raising operational and sustainability concerns.

Because the Competition Index is constructed from relocation activity, it may be endogenous to local demand conditions and operator strategy. Relocations can respond to anticipated demand, supply imbalance, rival presence, and service-quality targets, while they can also influence subsequent availability and utilization. Reverse causality and omitted demand shocks therefore cannot be ruled out given the observational nature of the data. We interpret the Competition Index as an observational marker of competition-related operational intensity and present the SHAP results as conditional descriptive associations within the fitted models, rather than as causal effects.

A plausible operational interpretation consistent with scooter-market practice is that under rivalry operators may engage in defensive deployments or defensive relocations into contested areas to protect market presence. Such behavior can co-occur with local oversupply when demand is limited or volatile, which can be associated with higher idle energy consumption. This interpretation is presented as a plausible explanation of the observed co-variation rather than an identified mechanism.

Moreover, interaction effects with spatial context reveal that the influence of competition is modulated by urban geography. Competitive impacts on idle energy consumption are amplified in peripheral areas, where system robustness is lower, and demand is less stable. In contrast, central zones display greater resilience, likely due to consistently high demand mitigating the adverse effects of competitive relocations. This spatial disparity underscores the strategic importance for operators, particularly weaker ones, to exercise caution in peripheral regions, where competitive maneuvers may inadvertently escalate energy inefficiency.

Collectively, these insights point to a nuanced relationship between competitive dynamics and operational sustainability in shared e-scooter systems. Effective management of fleet size, strategic deployment, and competition intensity appears crucial not only for maintaining market share but also for minimizing unnecessary energy expenditure, which holds significant implications for both economic performance and environmental sustainability.

5.2. Before-after Analysis of Competitive and Exclusive Market Conditions

After Operator B exited the Parma market on July 24, a single-operator environment prevailed until the end of the observation period. We provide a descriptive comparison of the coexistence period and the subsequent single-operator period to summarize how observed idle energy consumption and operational patterns differ across these two windows. This comparison is descriptive and should not be interpreted as evidence of a competition effect.

As shown in Fig. 11, the blue series depicts aggregate data under coexistence, the green series reflects Operator A during coexistence, and the orange series represents Operator A under exclusive conditions. Fig. 11(a) indicates that, during exclusivity, more spatial units exhibit lower average idle energy consumption. Fig. 11(b) and 11(c) show that Operator A's fleet size and relocation frequency remain broadly similar across the two windows, suggesting that these aggregate operational indicators do not show large shifts across periods.

Fig. 12 illustrates the spatial distribution of average idle energy consumption under three market conditions. Fig. 12(a) reports pooled observations during coexistence, while Figures 12(b) and 12(c) focus on Operator A during coexistence and exclusivity, respectively. After Operator B exited, total scooters in operation in the market declined because Operator A did not expand its fleet to offset the exit. Holding other conditions fixed, a reduction in overall market supply is consistent with faster turnover in higher-activity zones and lower per-idle consumption in those zones. However, demand conditions are not directly observed and may also change over time, so these cross-period differences remain descriptive.

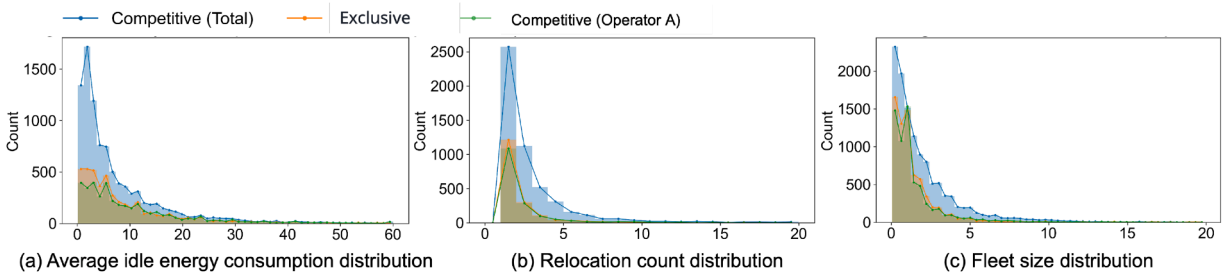

Fig. 11. Comparison of Data Distributions Under Competitive and Exclusive Market.

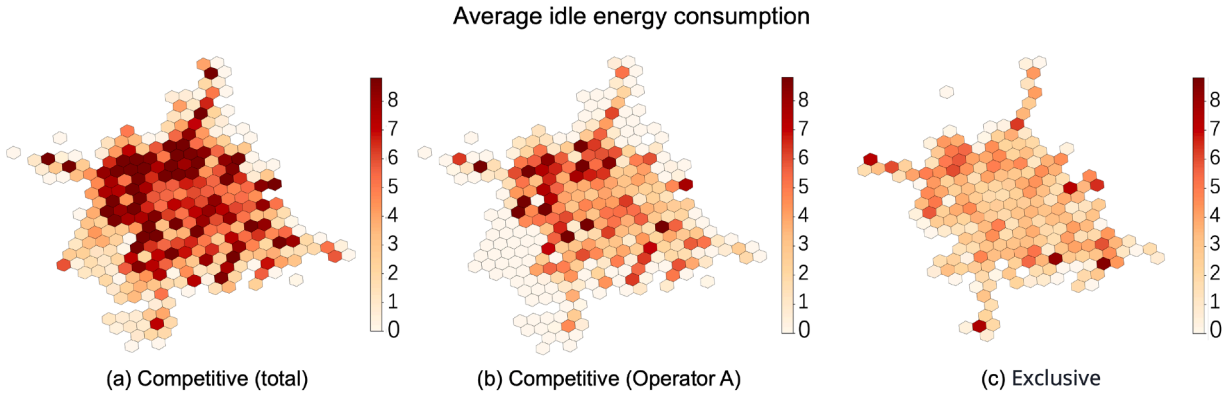

Fig. 12. Spatial Distribution of Idle Energy Consumption Under Competitive and Exclusive Market.

Comparing Figures 12(b) and 12(c) suggests lower average idle energy consumption for Operator A during exclusivity. This comparison should be interpreted cautiously, because the market configuration and total supply changed substantially over the same window, which makes direct efficiency comparisons across periods less straightforward.

A particularly noteworthy observation is a spatial shift in areas where Operator A exhibits high idle energy consumption. During the coexistence window, higher values are more visible in central areas, whereas during the subsequent single-operator window higher values are more visible in peripheral zones. This shift coincides with the change in market configuration and is consistent with the broader model-based evidence that competition-related patterns are more salient for the non-dominant operator and in peripheral or lower-activity contexts. At the same time, because the two windows occur at different times, other time-varying factors that affect demand distribution and turnover cannot be ruled out. We therefore interpret this hotspot shift as a descriptive pattern observed under two market configurations, rather than an isolated competition effect.

Other time-varying factors may also differ across the two windows and influence turnover and relocation needs, such as weather and shifts in travel demand over summer versus early autumn. For example, tourism and university schedules can change trip purposes, time-of-day profiles, and the spatial concentration of demand. A shift toward more leisure-oriented trips can disperse demand across recreational and visitor-oriented areas, while the resumption of academic and business activity can concentrate demand along specific corridors and around major activity centers. Such changes can alter where scooters experience long idle spells, how frequently they are repositioned, and which areas accumulate idle SOC depletion. Therefore, cross-period differences in idle energy consumption may reflect these time-varying demand patterns alongside the change in market configuration.

Consequently, the descriptive cross-period comparison remains potentially confounded by unobserved time-varying demand drivers. A clean adjustment for these factors would require multi-year high-resolution data. In shared e-scooter markets, operators frequently enter and exit, fleets and service areas change, and operating practices evolve over time. Even with multiple years of data, it is difficult to hold other determinants stable while isolating time-varying demand effects. Differences reported in this subsection should therefore be interpreted descriptively as patterns observed under different aggregate conditions, not as isolated causal effects of competition.

5.3. Policy and Operational Recommendations

The empirical results consistently indicate that operational inefficiency in idle states is linked to how competition is expressed through fleet deployment and relocation behavior, and that these links vary across space and across operators. The recommendations below translate these documented patterns into operational and regulatory actions, while keeping the interpretation within an associational scope.

First, the competition-index dependence shows a clear directional pattern: when the competition index is low, SHAP contributions for the competition index tend to be negative, while as competition intensity increases they become positive on average, indicating higher predicted idle energy consumption under more intense relocation-based rivalry (Fig. 9). This association is stronger for the non-dominant operator and is amplified in peripheral contexts (Fig. 10), where demand is less stable and the system is less resilient. In addition, the citywide classification suggests that benign competition is rare, whereas mild and harmful competition are widespread during the study window (Fig. 9). These results support operational rules that limit redundant relocation and repeated repositioning into low-turnover areas. For operators, this implies using demand-aware dispatch and relocation constraints to avoid cycles of defensive repositioning that increase idle exposure and idle depletion. For regulators, this supports targeted oversight of relocation intensity in highly contested areas, for example by monitoring relocation volumes and discouraging relocation practices that systematically generate oversupply without improving availability.

Second, the spatial results show pronounced heterogeneity across the city. Competition indicators and fleet sizes are highest in the city center and decline toward peripheral areas, while per-idle energy consumption is lower on average in central zones and higher in peripheral zones (Fig. 7). Exposure also varies substantially across space and time, as reflected by the idle-event count N^{u}_{idle}, which captures where idle spells are frequent and therefore where total idle losses can accumulate even when per-idle values are moderate. This combination of heterogeneity in competition, per-idle depletion, and exposure supports location-specific policies rather than uniform citywide rules. In dense central areas where demand and turnover are higher, operational constraints can focus on preventing oversupply and excessive deployment density. In peripheral areas where competition-related associations are stronger and per-idle depletion is higher, policies can prioritize reducing redundant relocations and stabilizing service levels. In the most sensitive peripheral zones, regulators can consider targeted permits, zone-based operating rules, or pilot interventions that reduce overlapping deployments and repeated relocations, while maintaining minimum service requirements.

Third, fleet size is a dominant contributor in the predictive models. In the overall SHAP summary, the fleet sizes of the two operators are the two most influential features, accounting for 36.9% and 28.2% of total within-model importance, and competition-related factors together account for 66.6% of total importance in the overall model (Fig. 8). The SHAP patterns also indicate that larger fleets are not consistently associated with lower predicted idle energy consumption, which is consistent with oversupply risks in some spatiotemporal units. This suggests that expanding fleet size alone does not guarantee improved energy efficiency. Operators should adopt demand-responsive fleet sizing strategies that adjust deployment scale to observed local turnover and predicted idle depletion patterns. Municipalities can support this by linking operating permits, fees, or fleet caps to operational-efficiency indicators, such as lower idle energy consumption per vehicle, while accounting for spatial context and avoiding one-size-fits-all thresholds.

Overall, the evidence indicates that sustainable e-scooter operations require managing competition intensity in relocation practices, recognizing spatial heterogeneity in demand and exposure, and adopting data-informed fleet strategies. Implementing these measures can reduce unnecessary idle depletion and improve both economic performance and environmental outcomes in shared micromobility systems.

6. Conclusion

This study examines how competition intensity is associated with idle energy consumption, an operational inefficiency that undermines the environmental and economic sustainability of micromobility systems. By leveraging high-resolution operational data from a dual-operator context in Parma, we developed a novel framework to capture the dynamic spatial interactions between operators. An interpretable machine learning framework was employed to model complex, non-linear relationships between competitive dynamics, contextual urban factors, and idle energy consumption.

The results show that idle energy consumption is strongly associated with the interplay between competition intensity, spatial context, and operator-specific strategies. Higher competition intensity, especially in low-demand peripheral areas, is associated with higher idle energy consumption, with weaker operators disproportionately affected. If left unmanaged, such dynamics can significantly undermine operational efficiency in shared e-scooter systems. Practically, the findings highlight the necessity for demand-responsive fleet management and informed regulatory interventions. Targeted policies and strategic deployment adjustments are warranted to mitigate energy inefficiencies and promote sustainable micromobility operations.

Despite these contributions, several limitations should be noted. First, our primary outcome is defined as the mean SOC loss per idle event (a conditional micro-scale measure). It does not directly represent the unit-level total idle energy burden, which also depends on exposure such as the number and duration of idle spells and the deployment scale. Complementary outcomes based on total idle SOC loss normalized by fleet size and/or time target a different estimand that blends exposure with per-spell severity and constitute an important extension for future work. The analysis focuses on a single urban context and a specific time window, which may limit the generalization of the findings to other cities or market configurations. The reason reflects the scarcity of open and comprehensive datasets. Within the study period, Parma was the only case where complete operational records were available, and where an operator exited, which allowed for a before-after comparison. Additionally, while the competition index effectively captures spatial relocation behavior, it does not encompass other strategic interactions, such as pricing or promotional campaigns. These factors are highly dynamic, since prices can fluctuate rapidly and marketing efforts are often short-term and irregular. This makes it challenging to track those factors systematically, yet they may also influence operational patterns and energy consumption

We acknowledge that several socioeconomic drivers, especially employment intensity, income, and other detailed demographic indicators, are not directly included in the main specification due to the lack of reliable public data at a granularity commensurate with our H3 grid in Parma. In the robustness check, we added a WorldPop population-density control as a coarse gridded proxy for local population intensity, but this variable cannot fully capture the broader socioeconomic structure of each cell. If these unobserved

factors correlate with both operator relocation strategies and idle-state energy consumption beyond what is captured by POIs, spatial location, transit accessibility, and population density, our results may still be subject to omitted variable bias.

Future research could address these gaps by extending the analytical framework to multi-city comparative studies, incorporating temporal dynamics over longer observation periods, and integrating richer data on operator strategies beyond spatial deployments. Further exploration of user behavior responses to competitive changes, as well as modeling of potential regulatory interventions, would also provide valuable insights into designing sustainable and efficient shared micromobility systems.

In conclusion, this study demonstrates that spatial competition is a critical and often overlooked correlate of idle energy consumption in shared e-scooter systems. By documenting the spatiotemporal patterns through which competitive dynamics are associated with operational efficiency, the findings contribute both theoretical and practical knowledge, offering pathways toward more sustainable and intelligently managed urban mobility networks.

CRediT authorship contribution statement

Yuhan Zhang: Writing – original draft, Visualization, Software, Methodology, Investigation, Formal analysis; **Jiaming Wu:** Writing – review & editing, Supervision, Funding acquisition, Data curation, Conceptualization; **Zhirui Ye:** Writing – review & editing, Supervision; **Maria Attard:** Writing – review & editing.

Data availability

Data will be made available on request.

Declaration of competing interest

The authors declare that they have no known competing financial interests or personal relationships that could have appeared to influence the work reported in this paper.

Acknowledgments

This work was supported by the project “Energy efficiency analysis for co-existing shared and electric micromobility systems,” funded by the Chalmers Area of Advance Energy, and the Swedish Energy Agency under project FEAT (P2022-00404). The authors also appreciate the support by the European Commission and VINNOVA through the DUT project ERGODIC (F-DUT-2022-0078).

References

Abouelela, M., Chaniotakis, E., Antoniou, C., 2023. Understanding the landscape of shared-e-scooters in north america; spatiotemporal analysis and policy insights. Transportation research part A: policy and practice 169, 103602.

Abouelela, M., Durán-Rodas, D., Antoniou, C., 2024. Do we all need shared e-scooters? an accessibility-centered spatial equity evaluation approach. Transportation Research Part A: Policy and Practice 181, 103985. https://doi.org/10.1016/j.tra.2024.103985

Al-Habaibeh, A., Watkins, M., Shakmak, B., Javareshk, M.B., Allison, S., 2024. Assessing air quality and physical risks to e-scooter riders in urban environments through artificial intelligence and a mixed methods approach. Applied Energy 376, 124282.

Badia, H., Jenelius, E., 2023. Shared e-scooter micromobility: review of use patterns, perceptions and environmental impacts. Transport reviews 43 (5), 811–837.

Bozzi, A.D., Aguilera, A., 2021. Shared e-scooters: A review of uses, health and environmental impacts, and policy implications of a new micro-mobility service. Sustainability 13 (16), 8676.

Breiman, L., 2001. Random forests. Machine learning 45, 5–32.

Budnitz, H., Li, X., Morrissey, H., Schwanen, T., 2025. Understanding the uneven use of rental e-scooters and implications for equity: Evidence from england’s largest e-scooter trial. Case Studies on Transport Policy 19, 101392. https://doi.org/10.1016/j.cstp.2025.101392

Cao, Z., 2025. Understanding how street environment affects e-scooter mode choice through travel experience. Cities 158, 105511. https://doi.org/10.1016/j.cities.2024.105511

Caspi, O., Smart, M.J., Noland, R.B., 2020. Spatial associations of dockless shared e-scooter usage. Transportation Research Part D: Transport and Environment 86, 102396.

Chen, S., Cao, Z., Zhang, X., 2025. Adaptive scootability index: Built environment, travel purpose and e-scooter preferred route. Journal of Transport Geography 123, 104117. https://doi.org/10.1016/j.jtrangeo.2025.104117

Contreras Pinochet, L.H., Pardim, V.I., Mangini, H., de Souza, C.A., 2025. Understanding the role of shared electric scooters in são paulo’s urban micromobility landscape. Case Studies on Transport Policy 20, 101419. https://doi.org/10.1016/j.cstp.2025.101419

Currie, G., Delbosc, A., Cox, R., Jayawardhena, M., Reynolds, J., 2025. Exploring shared e-scooter trip patterns and links to public transport service level. Multimodal Transportation 4 (2), 100205. https://doi.org/10.1016/j.multra.2025.100205

Electric-Scooter.Wiki Community, 2024. Lime scooter generations and specifications. Retrieved from https://electric-scooter.wiki/.

Emami, E., Ramezani, M., 2024. Integrated operator and user-based rebalancing and recharging in dockless shared e-micromobility systems. Communications in Transportation Research 4, 100155.

Fuady, S.N., Pfaffenbichler, P.C., Susilo, Y.O., 2024. Bridging the gap: Toward a holistic understanding of shared micromobility fleet development dynamics. Communications in Transportation Research 4, 100149.

Gioldasis, C., Christoforou, Z., Katsiadrami, A., 2024. Usage factors influencing e-scooter energy consumption: An empirical investigation. Journal of Cleaner Production 452, 142165. https://doi.org/10.1016/j.jclepro.2024.142165

Guo, Y., Zhang, Y., 2021. Understanding factors influencing shared e-scooter usage and its impact on auto mode substitution. Transportation research part D: transport and environment 99, 102991.

Heumann, M., Kraschewski, T., Brauner, T., Tilch, L., Breitner, M.H., 2021. A spatiotemporal study and location-specific trip pattern categorization of shared e-scooter usage. Sustainability 13 (22), 12527.

Hollingsworth, J., Copeland, B., Johnson, J.X., 2019. Are e-scooters polluters? the environmental impacts of shared dockless electric scooters. Environmental Research Letters 14 (8), 084031.

Hu, L., Liao, Y., Gao, K., Jin, S., Precup, R.-E., 2025. Integration of e-scooter sharing with public transit on employment accessibility and equity. Transportation Research Part D: Transport and Environment 140, 104604. https://doi.org/10.1016/j.trd.2025.104604
Hu, Y., Zhao, M., Zhao, Z., 2024. Uncovering heterogeneous effects of link-level street environment on e-bike and e-scooter usage. Transportation Research Part D: Transport and Environment 136, 104477. https://doi.org/10.1016/j.trd.2024.104477
Huang, E., Yin, Z., Broaddus, A., Yan, X., 2024. Shared e-scooters as a last-mile transit solution? travel behavior insights from los angeles and washington DC. Travel behaviour and society 34, 100663.
Huang, Y., Khajepour, A., Wang, H., 2016. A predictive power management controller for service vehicle anti-idling systems without a priori information. Applied Energy 182, 548–557.
Huo, J., Yang, H., Li, C., Zheng, R., Yang, L., Wen, Y., 2021. Influence of the built environment on e-scooter sharing ridership: A tale of five cities. Journal of transport geography 93, 103084.
Inman, J., 1849. Navigation and nautical astronomy: For the use of British seamen. F. and J. Rivington.
Jiao, J., Xu, Y., Li, Y., 2024a. Exploring spatial heterogeneity of e-scooter's relationship with ridesourcing using explainable machine learning. Transportation Research Part D: Transport and Environment 136, 104452.
Jiao, J., Xu, Y., Li, Y., 2024b. Exploring spatial heterogeneity of e-scooter's relationship with ridesourcing using explainable machine learning. Transportation Research Part D: Transport and Environment 136, 104452. https://doi.org/10.1016/j.trd.2024.104452
Jin, S.T., Wang, L., Sui, D., 2023. How the built environment affects e-scooter sharing link flows: A machine learning approach. Journal of transport geography 112, 103687.
Karimi, S., Kluger, R., 2025. Urban micromobility and social equity: An investigation through the lens of shared e-scooter rebalancing. Research in Transportation Business & Management 61, 101418. https://doi.org/10.1016/j.rtbm.2025.101418
Kazemzadeh, K., Sprei, F., 2024. The effect of shared e-scooter programs on modal shift: Evidence from sweden. Sustainable Cities and Society 101, 105097. https://doi.org/10.1016/j.scs.2023.105097
Kim, M., Zo, H., Chiravuri, A., 2025. Understanding the role of shared e-scooters in seoul: The perspective of regional transportation system and commuting population. Travel Behaviour and Society 40, 101038. https://doi.org/10.1016/j.tbs.2025.101038
Kimpton, A., Loginova, J., Pojani, D., Bean, R., Sigler, T., Corcoran, J., 2022. Weather to scoot? how weather shapes shared e-scooter ridership patterns. Journal of Transport Geography 104, 103439.
Lee, G., Lee, J.S., Park, K.S., 2024. Battery swapping, vehicle rebalancing, and staff routing for electric scooter sharing systems. Transportation Research Part E: Logistics and Transportation Review 186, 103540.
Li, A., Gao, K., Zhao, P., Axhausen, K.W., 2024. Integrating shared e-scooters as the feeder to public transit: A comparative analysis of 124 european cities. Transportation Research Part C: Emerging Technologies 160, 104496. https://doi.org/10.1016/j.trc.2024.104496
Li, A., Zhao, P., Liu, X., Mansourian, A., Axhausen, K.W., Qu, X., 2022. Comprehensive comparison of e-scooter sharing mobility: Evidence from 30 european cities. Transportation Research Part D: Transport and Environment 105, 103229.
Lundberg, S.M., Lee, S.-I., 2017. A unified approach to interpreting model predictions. Advances in neural information processing systems 30.
McKenzie, G., 2019. Spatiotemporal comparative analysis of scooter-share and bike-share usage patterns in washington, DC. Journal of transport geography 78, 19–28.
Molnar, C., 2020. Interpretable machine learning. Lulu. com.
Osorio, J., Lei, C., Ouyang, Y., 2021. Optimal rebalancing and on-board charging of shared electric scooters. Transportation Research Part B: Methodological 147, 197–219.
Schumann, H.-H., Haitao, H., Natapov, A., Quddus, M., 2025. The influence of spatial configuration on e-scooter traffic flows. Transportation Research Part A: Policy and Practice 198, 104529. https://doi.org/10.1016/j.tra.2025.104529
Segway Inc., 2020. Segway Ninebot ES4 KickScooter Specifications. Product specification sheet, retrieved from https://www.segway.com/.
Shah, N.R., Ziedan, A., Brakewood, C., Cherry, C.R., 2023. Shared e-scooter service providers with large fleet size have a competitive advantage: Findings from e-scooter demand and supply analysis of nashville, tennessee. Transportation Research Part A: Policy and Practice 178, 103878. https://doi.org/10.1016/j.tra.2023.103878
Statista Research Department, 2025. Forecast: revenue in the e-scooter-sharing market worldwide 2017–2029. https://www.statista.com/statistics/1448200/e-scooter-sharing-market-revenue-forecast-worldwide/. Accessed: 2025-06-28.
Towards Automotive, 2025. Light electric vehicle market review, key business drivers and industry forecast. https://www.towardsautomotive.com/insights/light-electric-vehicle-market-sizing. Accessed: 2025-06-28.
Verma, P., McKenzie, G., 2024. Regional comparison of socio-demographic variation in urban e-scooter usage. Environment and Planning B: Urban Analytics and City Science 51 (7), 1548–1562.
Wang, Y., Wu, J., Chen, K., Liu, P., 2021. Are shared electric scooters energy efficient? Communications in Transportation Research 1, 100022.
Wu, Y., Liu, T., Du, B., 2024. Fleet sizing and static rebalancing strategies for shared e-scooters: A case study in indianapolis, USA. Transportation Research Part A: Policy and Practice 190, 104287. https://doi.org/10.1016/j.tra.2024.104287
Xiong, R., Cao, J., Yu, Q., He, H., Sun, F., 2017. Critical review on the battery state of charge estimation methods for electric vehicles. Ieee Access 6, 1832–1843.
Yan, X., Zhao, X., Broaddus, A., Johnson, J., Srinivasan, S., 2023. Evaluating shared e-scooters' potential to enhance public transit and reduce driving. Transportation research part D: transport and environment 117, 103640.
Yang, H., Bao, Y., Huo, J., Hu, S., Yang, L., Sun, L., 2022a. Impact of road features on shared e-scooter trip volume: A study based on multiple membership multilevel model. Travel Behaviour and Society 28, 204–213.
Yang, H., Zheng, R., Li, X., Huo, J., Yang, L., Zhu, T., 2022b. Nonlinear and threshold effects of the built environment on e-scooter sharing ridership. Journal of Transport Geography 104, 103453.
Yang, W., Ewing, R., 2024. Unlocking the role of shared dockless e-scooters bridging last-mile gaps: A quasi-experimental study of metro rail transit in los angeles. Travel Behaviour and Society 37, 100869.
Yang, Y., Saridakis, C., Wadud, Z., Kothawala, A., Jena, A., Ozbilen, B., Wang, K., Circella, G., Castellanos, S., Grant-Muller, S., 2025. Understanding factors influencing user retention in shared e-scooter schemes: A comparative study of the UK/EU and the US. Travel Behaviour and Society 41, 101067. https://doi.org/10.1016/j.tbs.2025.101067
Zhai, G., Wang, R., Liu, X., Mladenović, M.N., Tang, Y., Mu, H., Liu, X., Yang, H., 2025. Built environment impacts on zonal shared e-scooter expenses: A bayesian learning approach. Transportation Research Part D: Transport and Environment 148, 105020. https://doi.org/10.1016/j.trd.2025.105020
Zhang, W., Buehler, R., Broaddus, A., Sweeney, T., 2021. What type of infrastructures do e-scooter riders prefer? a route choice model. Transportation research part D: transport and environment 94, 102761.
Zhang, Y., Shao, Y., Bi, H., Aoyong, L., Ye, Z., 2023. Bike-sharing systems rebalancing considering redistribution proportions: A user-based repositioning approach. Physica A: Statistical Mechanics and its Applications 610, 128409.
Zhao, J., Wu, J., Fotedar, S., Li, Z., Liu, P., 2024. Fleet availability analysis and prediction for shared e-scooters: An energy perspective. Transportation Research Part D: Transport and Environment 136, 104425. https://doi.org/10.1016/j.trd.2024.104425
Zhu, R., Kondor, D., Cheng, C., Zhang, X., Santi, P., Wong, M.S., Ratti, C., 2022. Solar photovoltaic generation for charging shared electric scooters. Applied Energy 313, 118728.